UNIVERSIDADE ESTADUAL DE CAMPINAS
Faculdade de Engenharia Elétrica e de Computação

Maria Cecilia Luna Alvarado

Performance Evaluation of SOCA-CFAR detectors in Weibull-Distributed Clutter Environments

Análise de Desempenho de um Detector SOCA-CFAR em Ambientes Tipo Weibull

Campinas

2022

Maria Cecilia Luna Alvarado

Performance Evaluation of SOCA-CFAR detectors in Weibull-Distributed Clutter Environments

Análise de Desempenho de um Detector SOCA-CFAR em Ambientes Tipo Weibull

Dissertation presented to the School of Electrical and Computer Engineering of the University of Campinas in partial fulfillment of the requirements for the degree of Master in Electrical Engineering, in the area of Telecommunications and Telematics.

Dissertação apresentada à Faculdade de Engenharia Elétrica e de Computação da Universidade Estadual de Campinas como parte dos requisitos exigidos para a obtenção do título de Mestre em Engenharia Elétrica, na Área de Telecomunicações e Telemática

Supervisor: Prof. Dr. Yuzo Iano

Este trabalho corresponde à versão final da dissertação defendida pelo aluno Maria Cecilia Luna Alvarado, e orientada pelo Prof. Dr. Yuzo Iano.

Campinas

2022

Ficha catalográfica
Universidade Estadual de Campinas
Biblioteca da Área de Engenharia e Arquitetura
Rose Meire da Silva - CRB 8/5974

L971p

Luna Alvarado, Maria Cecilia, 1996-
Performance evaluation of SOCA-CFAR detectors in Weibull-distributed clutter environments / Maria Cecilia Luna Alvarado. – Campinas, SP : [s.n.], 2022.

Orientador: Yuzo Iano.
Dissertação (mestrado) – Universidade Estadual de Campinas, Faculdade de Engenharia Elétrica e de Computação.

1. Alvos de radar. 2. Radar de rastreio. 3. Radar - Interferência. 4. Radar - Modelos matemáticos. I. Iano, Yuzo, 1950-. II. Universidade Estadual de Campinas. Faculdade de Engenharia Elétrica e de Computação. III. Título.

Informações para Biblioteca Digital

Título em outro idioma: Análise de desempenho de um detector SOCA-CFAR em ambientes tipo Weibull
Palavras-chave em inglês:
Radar targets
Tracking radar
Radar interference
Radar - Mathematical models
Área de concentração: Telecomunicações e Telemática
Titulação: Mestra em Engenharia Elétrica
Banca examinadora:
Yuzo Iano [Orientador]
Euclides Lourenço Chuma
Kelem Christine Pereira Jordão
Data de defesa: 05-04-2022
Programa de Pós-Graduação: Engenharia Elétrica

Identificação e informações acadêmicas do(a) aluno(a)
- ORCID do autor: https://orcid.org/0000-0001-9352-3668
- Currículo Lattes do autor: http://lattes.cnpq.br/4105383250262285

COMISSÃO JULGADORA - TESE DE MESTRADO

Candidato(a): Maria Cecilia Luna Alvarado RA: 264371
Data de defesa: 05 de Abril de 2022
Título da Tese: "Análise de Desempenho de um Detector SOCA-CFAR em Ambientes Tipo Weibull"

Prof. Dr. Yuzo Iano (Presidente)
Dr. Euclides Lourenço Chuma
Dra. Kelem Christine Pereira Jordão

A Ata de Defesa, com as respectivas assinaturas dos membros da Comissão Julgadora, encontra-se no SIGA (Sistema de Fluxo de Dissertação/Tese) e na Secretaria de Pós-Graduação da Faculdade de Engenharia Elétrica e de Computação.

To my parents Wilmer and Cecilia. To my husband Lenin.

Acknowledgements

I thank God for allowing me to fulfil my dreams.

To my parents and my sister, for their love and support.

To my husband for being my inspiration.

I would like to thank Prof. Yuzo Iano, for his guidance and support through my studies and for allowing me the opportunity to carry out my master's studies in this prestigious university.

To my friends Gabriela, Diana, Byron, Karen, Levy, and Rony for their unconditional friendship and help during my stay in Brazil. My special thanks to my friend and colleague Fernando for his valuable guidance and knowledge.

This study was finance in part by the Coordenação de Aperfeiçoamento de Pessoal de Nível Superior - Brasil (CAPES) - Finance Code 001.

"The sky is and has always been a pluralistic marketplace of human ideas and dreams"
(David Dickinson)

Resumo

Neste trabalho, derivamos uma nova expressão exata para a probabilidade de falso alarme (PFA) e uma solução aproximada de forma fechada para a probabilidade de detecção (PD) do detector *smallest of cell-averaging constant false alarm-rate* (SOCA-CFAR), operando sobre *clutter* do tipo Weibull. Para a análise, consideramos um alvo distribuído exponencialmente e consideramos valores arbitrários para o parâmetro de forma do *clutter*. Até onde sabemos, não existem avaliações de desempenho exatas nem aproximadas para um detector SOCA-CFAR considerando valores arbitrários para o parâmetro de forma das amostras de interferência Weibull (i.e., diferente de 1) contidas na janela CFAR. Portanto, nossas derivações analíticas generalizam estudos anteriores de avaliação de desempenho e dão um grande passo em direção a uma melhor compreensão de detectores SOCA-CFAR mais realistas. Além disso, obtemos formulações exatas para a função de densidade de probabilidade (PDF) e a função de distribuição cumulativa (CDF) para o mínimo de duas somas de variáveis aleatórias Weibull independentes e identicamente distribuídas (i.i.d.). Os resultados numéricos indicam que o desempenho do sistema melhora à medida que o parâmetro de forma da interferência aumenta. A validade de todas as nossas expressões é confirmada por meio de simulações de Monte Carlo.

Palavras-chaves: Smallest of cell-averaging constant false alarm-rate (SOCA-CFAR); probabilidade de detecção (PD); probabilidade de falso alarme (PFA); clutter do tipo Weibull.

Abstract

In this work, we derive a novel exact expression for the probability of false alarm (PFA) and an approximate closed-form solution for the probability of detection (PD) of a smallest of cell-averaging constant false alarm rate (SOCA-CFAR) detector operating over Weibull-distributed clutter. For the analysis, we consider an exponentially distributed target and allow arbitrary values for the shape parameter of the clutter interference. To the best of our knowledge, there are no exact nor approximate performance evaluations for a SOCA-CFAR detector considering arbitrary values for the shape parameter of the Weibull interference samples (i.e., different from 1) contained within the CFAR window. Therefore, our analytical derivations generalize previous performance evaluation studies and take a considerable step towards a better understanding of more realistic SOCA-CFAR detectors. Moreover, we obtain exact formulations for the probability density function (PDF) and the cumulative distribution function (CDF) for the minimum of two sums of independent and identically distributed (i.i.d.) Weibull random variables. Numerical results indicate that the system performance improves as the shape parameter of the Weibull interference increases. The validity of all our expressions is confirmed via Monte Carlo simulations.

Keywords: Smallest of cell-averaging constant false alarm-rate (SOCA-CFAR); probability of detection (PD); probability of false alarm (PFA); Weibull-distributed clutter.

List of Figures

Figure 2.1 – Major elements of a radar's system. 23
Figure 2.2 – PDFs associated with H_0 and H_1. 26
Figure 2.3 – Possible errors in hypothesis testing with their associated probabilities. 26
Figure 2.4 – Trading error by varying the threshold. 27
Figure 3.1 – The (a) PDF and (b) CDF of the exponential distribution for various values of η. 30
Figure 3.2 – The (a) PDF and (b) CDF of the Rayleigh distribution for multiple values of ρ. 31
Figure 3.3 – The (a) PDF and (b) CDF of the Chi-squared distribution for multiple values of ν. 33
Figure 3.4 – The (a) PDF and (b) CDF of the Weibull distribution with $\lambda = 2$ for multiple values of k. 34
Figure 3.5 – The (a) PDF and (b) CDF of the log-normal distribution with $\sigma = 0.4$ and for multiple values of μ. 35
Figure 4.1 – Generic architecture of a CFAR detector. 36
Figure 5.1 – PDF of Z for multiple values of N. 44
Figure 5.2 – CDF of Z for multiple values of N. 44
Figure 5.3 – PDF of $\alpha - \mu$ distribution for multiple values of α, μ and with $\Omega = \sqrt{\mu/4}$. 47
Figure 5.4 – CDF of $\alpha - \mu$ distribution for multiple values of α, μ and with $\Omega = \sqrt{\mu/4}$. 47
Figure 6.1 – PDF of Y considering $k = 1.3$, $\lambda = 0.7$, and different values of N. . . . 51
Figure 6.2 – CDF of Y considering $k = 1.3$, $\lambda = 0.7$, and different values of N. . . . 51
Figure 6.3 – Probability plot of (5.21) versus the simulated CDF of Φ with distribution parameters $\hat{\eta} = 0.5$, $\hat{k} = 1.3$, $\hat{\lambda} = 0.7$ and estimated parameters $\alpha = 0.70$, $\mu = 3.38$, and $\Omega = 1.87$. 52
Figure 6.4 – Approximated PDF (5.20) versus simulated PDF of Φ for multiple values of parameters $\hat{\eta}$, $\hat{k}$, and $\hat{\lambda}$. 53
Figure 6.5 – PD versus PFA with $\hat{k} = 20$, $\hat{\lambda} = 6$, $\hat{\eta} = 12$, and considering $k = 2$, $\lambda = 1$ for multiple values of N. 53
Figure 6.6 – PD versus PFA with $\hat{k} = 20$, $\hat{\lambda} = 6$, $\hat{\eta} = 12$, and considering $N = 1$, $\lambda = 1$ for different values of k. 54

List of Tables

Table 1.1 – Radar History Timeline 18
Table 1.2 – Nominal radar frequency bands (RICHARDS, 2014). 19
Table 1.3 – Radar applications. 20
Table 3.1 – Clutter versus Noise (RICHARDS et al., 2010). 29
Table 3.2 – Swerling Models (RICHARDS et al., 2010). 29
Table 4.1 – CFAR algorithms and the environment each one is design to operate in (RICHARDS et al., 2010). 39
Table 6.1 – Kolmogorov-Smirnov goodness-of-fit test for (5.20). 52

List of Acronyms

CA-CFAR	cell averaging constant false alarm rate
CDF	cumulative distribution function
CFAR	cell averaging constant false alarm rate
CUT	cell under test
CW	continuous wave
EM	electromagnetic
EMI	electromagnetic interference
GMM	generalized method of moments
GOCA-CFAR	greatest-of cell averaging constant false alarm rate
HF	high-frequency
HFSWR	high-frequency surface-wave radars
i.i.d.	independent and identically distributed
MLE	maximum-likelihood estimator
MM	method of moments
MTI	moving target indication
NP	Neyman-Pearson
NRL	U.S. Naval Research Laboratory
OS-CFAR	order statistics constant false alarm rate
PD	probability of detection
PDF	probability density function
PFA	probability of false alarm
RCS	radar cross section
RF	radio-frequency
RV	random variable
SAR	synthetic aperture radar
SNR	signal-to-noise ratio
SOCA-CFAR	smallest-of cell averaging constant false alarm rate
SW0	Swerling 0

SW1	Swerling 1
SW2	Swerling 2
SW3	Swerling 3
SW4	Swerling 4
TMLE	truncated-maximum-likelihood estimator
WGN	white Gaussian noise
WWII	World War II

List of Symbols

$\Gamma(\cdot)$	gamma function
$\Gamma(\cdot,\cdot)$	upper incomplete gamma function
$\gamma(\cdot,\cdot)$	lower incomplete gamma function
$\operatorname{erf}(\cdot)$	Gauss error function
$f_{(\cdot)}(\cdot)$	probability density function of a generic random variable
$F_{(\cdot)}(\cdot)$	cumulative distribution function of a generic random variable
$\Pr[\cdot]$	probability of an event
$\mathbb{E}[\cdot]$	expectation
$\mathbb{V}[\cdot]$	variance
$\lvert\cdot\rvert$	absolute value
${}_2F_1(\cdot,\cdot;\cdot;\cdot)$	Gauss hypergeometric function

Contents

1 INTRODUCTION 17
1.1 Radar Basics 17
1.1.1 Radar Basic Functions 20
1.1.2 Radar Applications 20
1.2 Some Basic Probability Concepts 21
1.2.1 Continuous Random Variable 21
1.2.2 Cumulative Distribution Function 21
1.2.3 Probability Density Function 21
1.2.4 Expected Value 22
1.2.5 Variance and Standard Deviation 22

2 DETECTION FUNDAMENTALS 23
2.1 Detection Theory 23
2.1.1 Neyman-Pearson Theorem 24
2.2 Radar Cross Section 26
2.3 Fluctuating Targets 27

3 RADAR SIGNAL MODELING 28
3.1 Noise and Clutter Modeling 28
3.2 Target Modeling 29
3.3 Related Distributions 29
3.3.1 Exponential Distribution 29
3.3.2 Rayleigh Distribution 30
3.3.3 Chi-square Distribution 32
3.3.4 Weibull Distribution 32
3.3.5 Log-normal Distribution 32

4 CONSTANT FALSE ALARM RATE 36
4.1 Cell Averaging CFAR 37
4.2 Greatest-of CA-CFAR 37
4.3 Smallest-of CA-CFAR 38
4.4 Censored CFAR 38
4.5 Order Statistics CFAR 38

5 SOCA-CFAR DETECTOR PERFORMANCE IN WEIBULL-DISTRIBUTED CLUTTER 40

5.1 Preamble . . . 41
5.2 Preliminaries . . . 42
5.2.1 Sum of i.i.d. Weibull variates . . . 43
5.3 Some Important Statistics . . . 43
5.3.1 Minimum of Two Sums of i.i.d. Weibull variates . . . 43
5.3.2 Clutter-Plus-Target Statistics . . . 45
5.4 The $\alpha - \mu$ Distribution . . . 46
5.5 SOCA-CFAR Detection . . . 47
5.5.1 SOCA-CFAR Performance Analysis . . . 48

6 RESULTS AND DISCUSSION . . . 50
6.1 Software . . . 50
6.2 Monte-Carlo Simulations . . . 50
6.3 Numerical Results . . . 50

7 CONCLUSIONS . . . 55

8 FUTURE WORKS . . . 56

BIBLIOGRAPHY . . . 57

APPENDIX 61

APPENDIX A – ABSOLUTE CONVERGENCE OF EQUATION (2.29) 62

APPENDIX B – ABSOLUTE CONVERGENCE OF EQUATION (2.33) 65

1 Introduction

This dissertation presents novel contributions in the scope of modern radar systems. More specifically we derive closed-form formulations that aid in the performance analysis of a constant false alarm detector. Our analysis considers that the clutter follows a Weibull distribution since many studies have demonstrated that it accurately describes realistic sea and ground clutter.

Before engaging the contributions we briefly review indispensable theoretical foundation on radar signal processing.

The remainder of this dissertation is organized as follows. Chapter 1 briefly introduces the radar concept as well as probability theory that is used throughout the work. Chapter 2 revisits essential notion regarding detection theory. Chapter 3 introduces the statistical model of clutter and target signals. Chapter 4 presents the constant false alarm rate (CFAR) concept as well as some of the primarily algorithms found in literature. Chapter 5 derives new formulations for the performance metrics of a smallest-of cell averaging constant false alarm rate (SOCA-CFAR) detector operating over Weibull clutter in an exact manner for probability of false alarm (PFA) and approximated for probability of detection (PD). Chapter 6 discusses the numerical results. Finally, conclusions and future works are presented in Chapters 7 and 8.

1.1 Radar Basics

Originally the word *radar* stood for *radio detection and ranging* since in its early developments radar systems were restricted to detection and range determination of targets. Nowadays, radar functions have expanded to search, track and image targets while suppressing undesired background interference. As well known, radars are electrical systems that transmit radio-frequency (RF) electromagnetic (EM) waves to a specific region to then receive the reflected signal and apply it to the receiver circuits. The major subsystems composing a radar include transmitter, antenna, receiver and signal processor (RICHARDS et al., 2010). A timeline of radar history and developments is shown in Table 1.1 (SKOLNIK, 2001).

1886	Hertz demonstrated that radio waves can be reflected by metallic objects and refracted by a dielectric prism
1900	Tesla conceptualize the detection and velocity measurement of EM waves

1904	Hülsmeyer tested ship detection by radio wave reflection
1922	Taylor and Young of the U.S. Naval Research Laboratory (NRL) proved ship detection by radar
	Marconi (pioneer of wireless radio) observed the radio detection of targets
1925	The pulse radar technique was used by Briet and Tuve of the Carnegie Institution in Washington D.C to measure the height of the ionosphere
1930	The NRL first detected and aircraft by radar
1934	The NRL research lead to a U.S. patent for *continuous wave* (CW) radar
	The NRL began serious efforts of developing pulse radar systems
1936	First successful demonstrations of the NRL pulse radar
	U.S Army Signal Corps begin active radar work
1938	The first U.S. Army Signal Corps operational radar system, the SCR-268 antiaircraft fire control system
	The operational shipboard radar Seetakt was installed by German Navy ships making Germany be ahead in radar technology.
1939	Second operational system the SCR-270, an early warning system which detections where ignored at Pearl Harbor
	British build their first 200 MHz airborne interceptor radar
	German Air Force produce the 125 MHz Freya air search and employed it as Ground Control of Intercept radar
1940	The British made a significant advance in radar technology by inventing the high-power microwave magnetron
	United States and Britain development of radars that operate at microwave frequencies (that have predominated since)

Table 1.1 – Radar History Timeline

As mentioned in the timeline, nowadays, conventional radars operate in the microwave region. The first radars operate in frequencies raging from 100 MHz to 36 GHz. Operational high-frequency (HF) over-the-horizon radars operate at MHz frequencies. On

the other hand, experimental millimeter wave radars operate at frequencies higher tan 240 GHz. During World War II (WWII), letters such as S, X L where use to designate frequency bands for radar operation with the purpose to maintain military secrecy. Since the shorthand designation was convenient for denoting the spectrum region in which the radar operates it is still in use (SKOLNIK, 2001). Table 1.2 presents the nominal radar frequency bands with its letter nomenclature.

During WWII radar technology grew rapidly and in the years that followed the war radar capability has continue to advance. Here are listed some of the major accomplishments of radar

- Usage of doppler effect in the moving target indication (MTI) pulse radar to separate targets from ground echoes.
- High-power stable amplifiers to allow better application of the doppler effect and much higher power than the obtained with the magnetron.
- Monopulse radar allow for highly accurate angle tracking of targets.
- The airborne synthetic aperture radar (SAR) to provide high resolution map-like imaging of ground scenes.
- Phase array antennas offer rapid beam direction without any mechanical movement of the antenna.
- Extracting information from the echo signal to provide target recognition.
- Radar has become an essential tool for meteorologist.

Table 1.2 – Nominal radar frequency bands (RICHARDS, 2014).

Band	Frequency
HF	3-30 MHz
VHF	30-300 MHz
UHF	300 MHz-1 GHz
L	1-2 GHz
S	2-4 GHz
C	4-8 GHz
X	8-12 GHz
Ku	12-18 GHz
K	18-27 GHz
Ka	27-40 GHz
mm	40-300 GHz

1.1.1 Radar Basic Functions

The bast majority of radars operate under three main functions which are: search, track and image. Such functions are described bellow (RICHARDS et al., 2010).

- Search: A radar searches a given volume for targets without a priori knowledge about targets' presence or position. To do so, the radar points its antenna in a series of beam positions transmitting one or more pulses. The received data is examined for the presence of targets using threshold techniques (described in Section 2).
- Track: When a target is detected a measurement of its state is performed and includes: azimuth and elevation angle, position in range. Then, all individual measurements are combined to estimate a target track.
- Image: Imaging refers to a variety of methods used to obtain detail information of broad-areas or discrete targets. The two processes involved in imaging are producing high-resolution range and cross-range profile of the target.

1.1.2 Radar Applications

Even thought early radar advancement was driven by military necessity (surveillance, navigation, weapon guidance), nowadays radar enjoys increasing civilian range of applications (police traffic radar, color weather radar, meteorological radar, aviation, i.a.). Table 1.3 shows some of the most common applications of radar technology (RICHARDS et al., 2010).

Table 1.3 – Radar applications.

Military Applications	Air traffic control Air defence systems Over-the-horizon search radars Ballistic missile defense radars Artillery locating radars Instrumentation test range radars Tracking, fire control, and missile support radars
Civilian Applications	Process control radars Airport surveillance radars Weather radars Navigation radars Satellite mapping radars Automotive collision avoidance radars Radar altimeters

1.2 Some Basic Probability Concepts

In this section we review some essential probability notion that will aid us better comprehend the following dissertation work.

1.2.1 Continuous Random Variable

A continuous random variable (RV) X is define as function that maps an outcome ς from an experimental sample space $\mathcal{S}$ to a numerical sample space $\mathcal{S}_X$, which is a subset of the real line $\mathbb{R}$. In contrast to a discrete RV the $\mathcal{S}_X$ consists of an infinite and uncountable number of outcomes. Therefore, the possible outcomes of the RV are intervals that are uncountable infinite sets and thus the probabilities are assigned to intervals (KAY, 2006).

1.2.2 Cumulative Distribution Function

The cumulative distribution function (CDF) of a RV X is given by

$$F_X(x) = P(X \leq x), \tag{1.1}$$

and is define as the probability that the RV X, evaluated at x, will take values that are less than or equal to x. It is a continuous non-decreasing function (YATES; GOODMAN, 2014). The properties of the CDF are

1. $F_X(-\infty) = 0$
2. $F_X(\infty) = 1$
3. $\Pr[x_1 < X \leq x_2] = F_X(x_2) - F_X(x_1)$

1.2.3 Probability Density Function

As stated in (YATES; GOODMAN, 2014) the slope of the CDF at any point x indicates the probability that X is near x. The slope of the CDF is what we refer to as probability density function (PDF). The PDF of a RV X is given by

$$f_X(x) = \frac{\mathrm{d}F_X(x)}{\mathrm{d}x}. \tag{1.2}$$

The properties of the PDF are

1. $f_X(x) \geq 0 \; for \; all \; x$
2. $F_X(x) = \int_{-\infty}^{x} f_X(u)\,\mathrm{d}u$
3. $\int_{-\infty}^{\infty} f_X(x)\,\mathrm{d}x = 1$

1.2.4 Expected Value

The expected value of a RV X, also called the first moment and denoted by $\mathbb{E}[X]$ or μ_X, is the average value of the outcomes in a great number of experimental trials which in the continuous case is define as the following integral (YATES; GOODMAN, 2014)

$$\mathbb{E}[X] = \int_{-\infty}^{\infty} x f_X(x) \mathrm{d}x. \tag{1.3}$$

The properties of the expected value are

1. $\mathbb{E}[X - \mu_X] = 0$
2. $\mathbb{E}[aX - b] = a\mathbb{E}[X] + b$

where a and b are constants.

1.2.5 Variance and Standard Deviation

Both variance $\mathbb{V}[\cdot]$ and standard deviation σ are measures of dispersion. The variance describes the difference between a RV X and its expected value and its given by (YATES; GOODMAN, 2014)

$$\mathbb{V}[X] = \mathbb{E}[(X - \mu_X)^2]. \tag{1.4}$$

The standard deviation of X is the squared root of the variance and is denoted by

$$\sigma_X = \sqrt{\mathbb{V}[X]}. \tag{1.5}$$

2 Detection Fundamentals

In this chapter we revisit essential notion that will be used throughout this dissertation work.

2.1 Detection Theory

The simplest decision problem one could have is to determine whether a signal is present or not, which is the case in radar systems. In radar we aim for determining the presence or absence of a target. To do so, we transmit an EM pulse which if reflected by the object, will indicate the presence of a target. Thus, the received waveform will consist of the reflected pulse plus thermal noise present at the receiver's circuits, conversely only noise will be present (RICHARDS et al., 2010). An example of this is presented in Figure 2.1 where the problem is the detection of an aircraft. This could be associated with a binary hypothesis testing problem since we wish to decide between two possible scenarios (KAY, 1998).

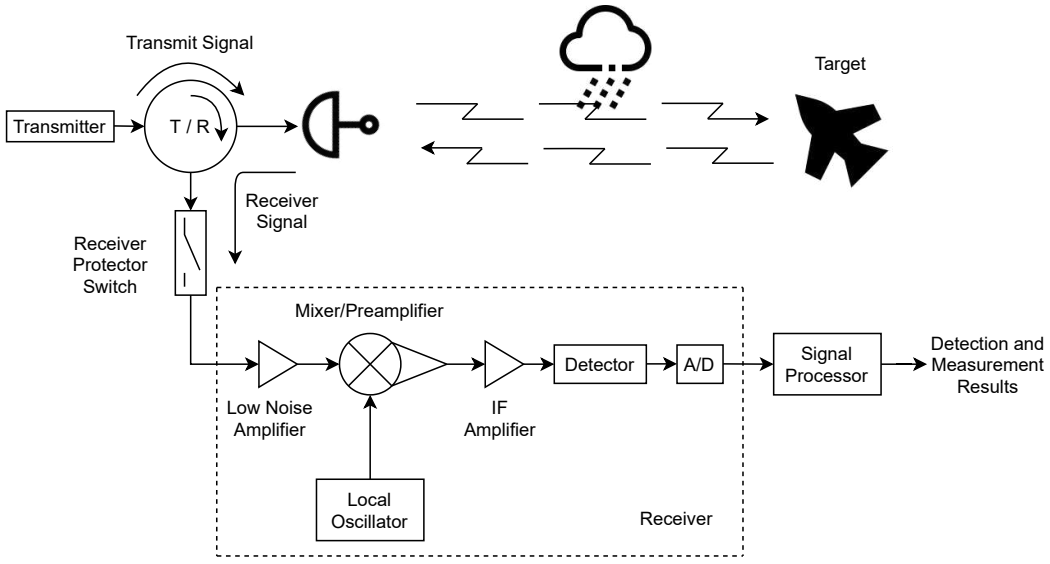

Figure 2.1 – Major elements of a radar's system.

To better illustrate the detection problem we exemplify the detection of a DC level of amplitude $A = 1$ embedded in white Gaussian noise (WGN) $w[n]$ using s single sample as in (KAY, 1998). We wish to decide between two hypothesis: noise only $x[0] = w[0]$ and signal embedded in noise $x[0] = 1 + w[0]$. Since the noise is assumed zero mean, for noise only $\mathbb{E}[x[0]] = 0$ and for a signal embedded in noise $\mathbb{E}[x[0]] = 1$, it is

reasonable to presume that a signal is present if

$$x[0] > \frac{1}{2} \tag{2.1}$$

or, that only noise is present if

$$x[0] < \frac{1}{2}. \tag{2.2}$$

It is evident that although we can not always make the correct decision it is important that most of the time we do. Hence, we wish to increase the signal-to-noise ratio (SNR), namely, increase "distance" between the PDFs associated with each hypothesis. This will lead to less incorrect decisions being made improving the detector's performance (KAY, 1998). A formal modeling for the previous problem will be choosing between H_0 which refers to the noise only hypothesis and H_1 which corresponds to the signal plus noise hypothesis, symbolically

$$\begin{aligned} H_0 : &\quad x[0] = w[0] \\ H_1 : &\quad x[0] = 1 + w[0]. \end{aligned} \tag{2.3}$$

In practice detecting a signal is more complex than the previous presented scenario since, generally, the signals we are interested in detecting are weak or have a small SNR. To overcome this we use multiple data samples in which to base our decision so that we depend on data record length (KAY, 1998). The previous DC problem will know be expressed as

$$\begin{aligned} H_0 : &\quad x[n] = w[n] \qquad\quad n = 0, 1, ..., N-1 \\ H_1 : &\quad x[n] = A + w[n] \qquad n = 0, 1, ..., N-1, \end{aligned} \tag{2.4}$$

where $w[n]$ is WGN with variance σ^2. As in (2.1), in which we used a single sample, we wish to define a rule for decision making. Therefore, it seems reasonable to first average the samples to then compare the obtained value (M) with a threshold τ. Here (2.1) is a special case with $N = 1$ and $\tau = 1/2$. Hence, we will accept H_1 as true if

$$M = \frac{1}{N} \sum_{n=0}^{N-1} x[n] > \tau. \tag{2.5}$$

To summarize the above, detection decisions are based on comparing reflected signals to a threshold to then choose between two hypothesis. Measurements surpassing the threshold are declare to contain echoes from targets embedded in interference and are related with target-plus-interference hypothesis (H_1). Conversely, measurements bellow the threshold are declare to contain only energy of interfering sources and are related with the null hypothesis (H_0).

2.1.1 Neyman-Pearson Theorem

As mentioned, every radar measurement is examined for the presence of a target and therefore one of two hypothesis can be presumed true:

1. Measurement that contains interference only, H_0.

2. Measurement containing echoes from a target embedded in interference, H_1.

Therefore, we need a criterion that aids us choose the optimal hypothesis. In radar the Neyman-Pearson (NP) theorem is the most commonly used approach for decision making. As in (KAY, 1998), with the following example we will address this approach for signal detection.

Assume we have an experiment in which we observe the realization of a RV with a Gaussian PDF, denoted by $\mathcal{N}(\mu, \sigma^2)$, where the mean parameter is either $\mu = 0$ or $\mu = 1$ and $\sigma^2 = 1$. For simplicity we are going to determine the value of μ based on a single observation $x[0]$. Each possible value of μ can be thought as a hypothesis and therefore we have the following binary hypothesis test

$$\begin{aligned} H_0 : &\quad \mu = 0 \\ H_1 : &\quad \mu = 1, \end{aligned} \tag{2.6}$$

where H_0 is referred to as the null hypothesis and H_1 as the alternative hypothesis. The PDFs associated with each hypothesis are shown in Figure 2.2, and as depicted the difference in means cause the PDF associated with H_1 to be shifted to the right.

As mentioned in Section 2.1 a reasonable approach will be to decide H_1 if $x[0] > 1/2$ because the area under the curve to the right of the dotted black line placed at $1/2$ is greater for H_1 than for H_0 and therefore is more likely for H_1 to be true. The detector will then compare the data with $1/2$ to which we refer as threshold. It is important to note that with this scenario the following errors may arise

- Type I error: deciding for H_1 when H_0 is true.
- Type II error: deciding for H_0 when H_1 is true.

Figure 2.3 depicts these errors where the notation $P(H_i|H_j)$ indicates the probability of deciding H_i when in fact H_j is true. These errors are unavoidable and as shown in Figure 2.4 we can only reduce one error at the expense of increasing the other by changing the threshold value, therefore, it is not possible to reduce both error probabilities at the same time.

In order to design an optimal detector it is a common approach to fix one error probability while attempting to minimize the other. Typically, we restrict $P(H_1|H_0)$, which is referred to as probability of false alarm (PFA), to a fixed small value α (e.g. 10^{-4}, 10^{-5}, 10^{-6}). Now we seek to minimize the other error $P(H_0|H_1)$ or equivalently maximize $1 - P(H_0|H_1)$ which is the same as $P(H_1|H_1)$ and in signal detection is called probability of detection (PD). This approach is known as the NP criterion for signal detection.

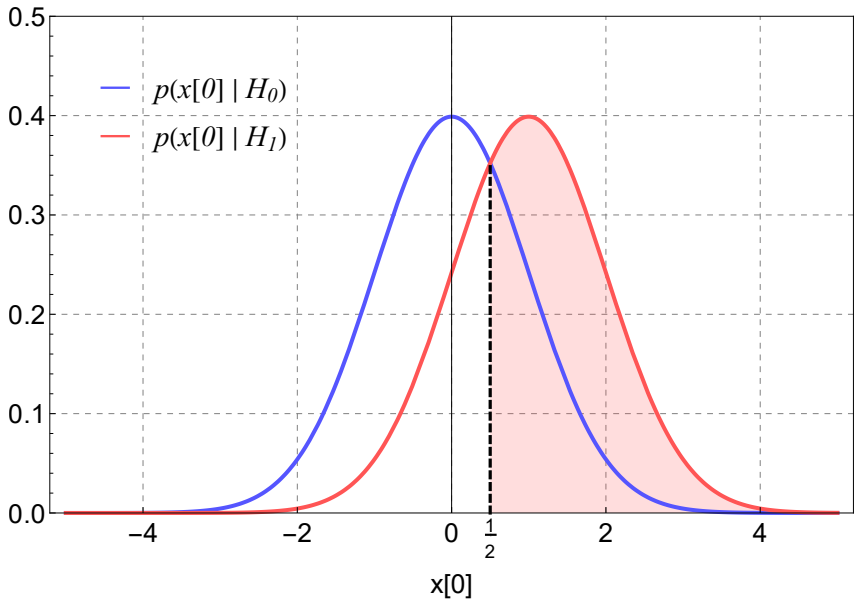

Figure 2.2 – PDFs associated with H_0 and H_1.

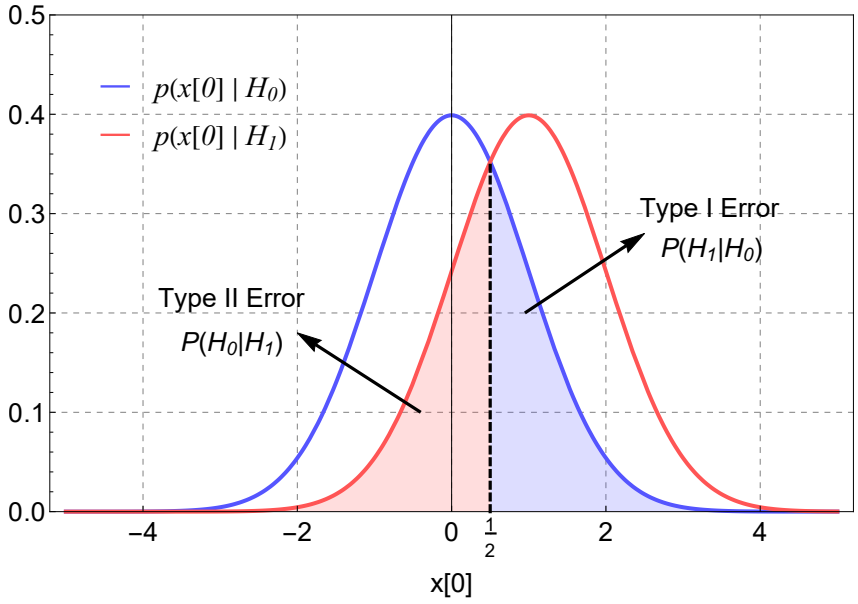

Figure 2.3 – Possible errors in hypothesis testing with their associated probabilities.

2.2 Radar Cross Section

Radar cross section (RCS) refers to the area θ of a target that reflects back isotropically and would have cause the same power return as the original target. Note that θ does not refer to a physical cross-section area of the target but to an equivalent area used to relate incident (at the target) and reflected (at the receiver) power density. It is intended to characterize the target and it is a function of several of its attributes (RICHARDS et al., 2010; RICHARDS, 2014; LEVANON, 1988), specifically

- Targets' geometry and material

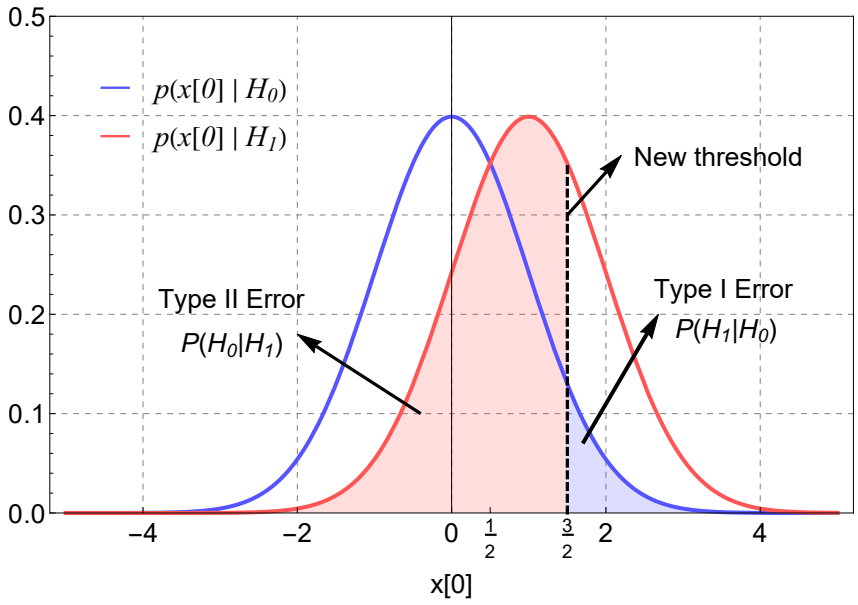

Figure 2.4 – Trading error by varying the threshold.

- Transmitter and receiver location relative to target
- Frequency of wavelength
- Transmitter and receiver polarization

2.3 Fluctuating Targets

The RCS of real targets can not be adequately modeled by a constant, generally, it is a complex function of frequency, polarization and aspect angle. Since the received power at the radar is proportional to the target's RCS, fluctuations in RCS lead to received target power fluctuations.

A fluctuating targets' RCS varies severely with respect to aspect angle or frequency. This behaviour is observed even in lessen complex targets leading to performance analysis computations that are highly dependent on radar-target aspect angle and SNR. Since it is difficult to know the RCS accurately enough the calculations become complex and of limited utility. Thus, it is more useful to develop simpler models of target RCS which leads to the use of RVs with a specified PDF to describe the composite RCS of the scatterers.

3 Radar Signal Modeling

The fundamental problem in radar systems relies in determining whether the signal measured at the radar's receiver represents echo from a target or noise only. It is important to note that the noise is always present at the receiver and therefore the received target signals is embedded in noise. The unwanted noise can occur as a result of internal and external electronic noise, reflected EM waves from other objects called clutter (e.g. surfaces on the ground or in the atmosphere), sources of electromagnetic interference (EMI) or intentional jamming (RICHARDS et al., 2010).

The detection performance of a radar system depends on our knowledge of signal and noise characteristics in terms of their PDFs (KAY, 1998). Therefore, it is important that we have exact or at least accurate knowledge of the PDFs so the false alarm rate would decrease. Thus, we need models that better describe the target, noise and clutter.

Depending on the source the interference can be classified as noise or clutter, both presenting a randomly varying voltage at the receiver's output. The target also presents a random varying voltage due to the multiple scatterers. Because of its different origin nature, noise, clutter and target are modeled by different PDFs. The stochastic nature of both the target-plus-clutter and clutter signals require the detection process of a radar to be specified in terms of PD and PFA. The likelihood of detecting a target is associated with PD, whereas PFA is understood as the fraction of detection test in which a false alarm occurs (RICHARDS et al., 2010).

3.1 Noise and Clutter Modeling

As mentioned noise and clutter are modeled differently primarily because each one exhibits specific properties. Table 3.1 summarizes the main differences between noise and clutter returns.

As seen, the major differences that clutter presents with respect to noise are: its power spectrum is not white (due to high correlation); and, since the clutter is an echo from the transmitted signal, its received power is affected by environmental and radar parameters (antenna gain, transmitted power, range from radar to terrain) making its characterization far more complex. Conversely, noise is affected by the radar's receiver noise figure and bandwidth (RICHARDS, 2014).

In radars, in order to analytically determine the PFA for a given noise its PDF ought to be known requiring knowledge of the noise statistics. For instance noise is

said to follow Rayleigh (for a linear detector) or exponential distributions (for a square law detector) while clutter is commonly modeled by Weibull (ground and sea clutter), log-normal (sea and weather clutter) and K distributions (sea clutter) (RICHARDS et al., 2010; SEKINE; MAO; MAO, 1990).

Table 3.1 – Clutter versus Noise (RICHARDS et al., 2010).

Noise Signal	Clutter Signal
Amplitude is independent of the transmitted radar signal	Amplitude is proportional to the transmitted signal
Wide bandwidth	Narrow bandwidth
Statistically independent between pulses	May be highly correlated between pulses
Independent of transmitted frequency	Varies with changing frequency
Independent of environmental parameters	Can vary with changing environmental conditions

3.2 Target Modeling

Among the many models available for target modeling we have a set of four statistical models, commonly refer to as Swerling models, that aids us describe different fluctuating conditions of targets each one having an specific fluctuation rate, see Table 3.2. A non-fluctuating target is termed as a Swerling 0 (SW0) (RICHARDS et al., 2010).

Table 3.2 – Swerling Models (RICHARDS et al., 2010).

Case	PDF	Fluctiation Period
SW1	Rayleigh	Dwell-to-Dwell
SW2	Rayleigh	Pulse-to-Pulse
SW3	Chi-square, degree 4	Dwell-to-Dwell
SW4	Chi-square, degree 4	Pulse-to-Pulse

3.3 Related Distributions

Here we briefly describe some of the distributions used for noise, clutter and target modeling as well as some of their applications.

3.3.1 Exponential Distribution

The exponential distribution is a single parameter distribution, commonly known as rate parameter (η). It describes the time between events in a Poisson process.

Its PDF and CDF are given by (FORBES et al., 2011):

$$f_X(x) = \eta \exp(-\eta\, x) \qquad x \geq 0 \tag{3.1}$$

$$F_X(x) = 1 - \exp(-\eta\, x) \qquad x \geq 0. \tag{3.2}$$

Among the multiple applications of the exponential distribution we have: time to decay of a radioactive atom, time to failure of components with constant failure rates and theory of waiting lines (FORBES et al., 2011). Figure 3.1 shows (a) the PDF and (b) CDF of the exponential distribution for multiple values of the rate parameter η.

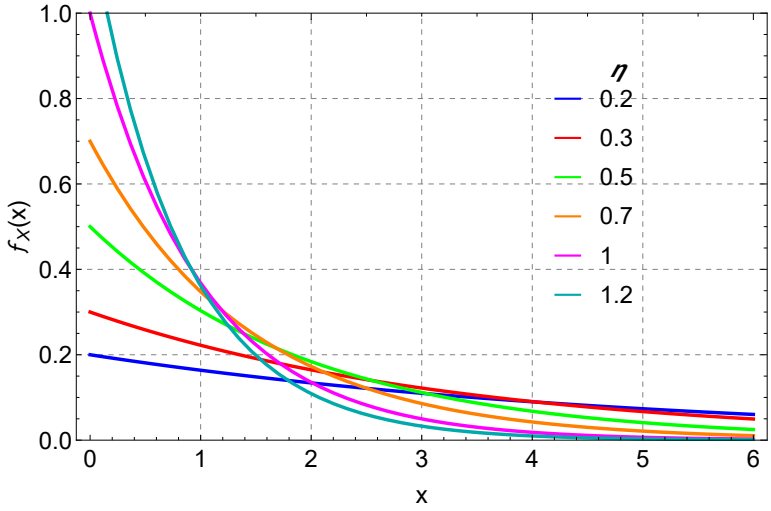

(a)

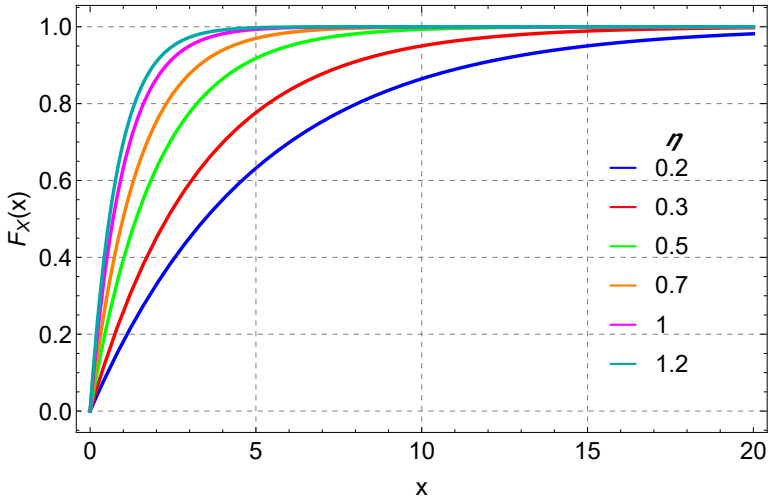

(b)

Figure 3.1 – The (a) PDF and (b) CDF of the exponential distribution for various values of η.

3.3.2 Rayleigh Distribution

The Rayleigh distribution is a one parameter distribution known as the scale parameter (ρ). If X follows a Rayleigh distribution, then X^2 has an exponential distribution

with rate parameter $2\rho^2$. Its PDF and CDF are given by (FORBES et al., 2011):

$$f_X(x) = \frac{x}{\rho^2} \exp\left(-\frac{x^2}{2\rho^2}\right) \qquad x \geq 0 \tag{3.3}$$

$$F_X(x) = 1 - \exp\left(-\frac{x^2}{2\rho^2}\right) \qquad x \geq 0. \tag{3.4}$$

One of its applications is physical oceanography since wave heights are usually modeled by a Rayleigh distribution (MACKAY, 2012). It is also used in the analysis of wind velocity (da Rosa; ORDóñEZ, 2022). Figure 3.2 shows (a) the PDF and (b) CDF of the Rayleigh distribution for multiple values of the scale parameter ρ.

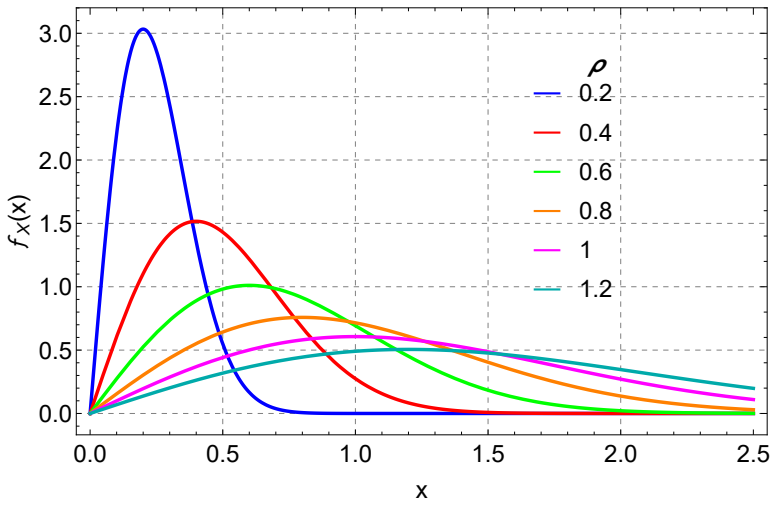

(a)

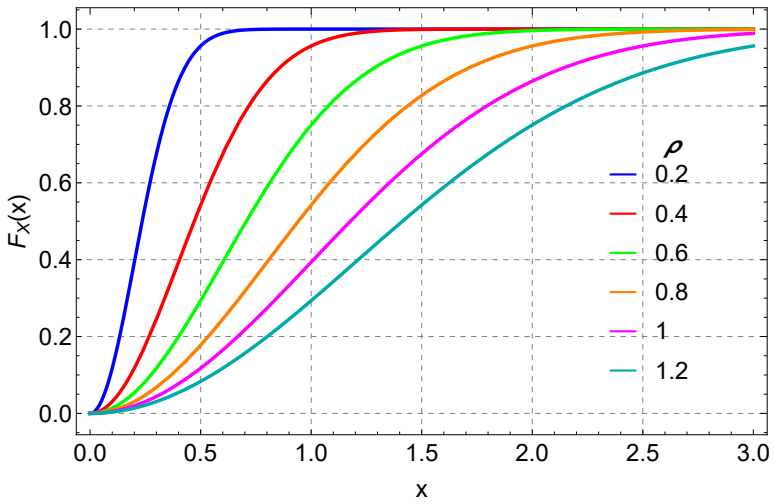

(b)

Figure 3.2 – The (a) PDF and (b) CDF of the Rayleigh distribution for multiple values of ρ.

3.3.3 Chi-square Distribution

It is the distribution of the sum of the squares of ν standard normal variates. It is commonly used in goodness-of-fit tests between observed data and theoretical distributions. Its PDF and CDF are given by (FORBES et al., 2011):

$$f_X(x) = \frac{x^{\frac{\nu}{2}-1} \exp\left(-\frac{x}{2}\right)}{2^{\nu/2}\,\Gamma\left(\frac{\nu}{2}\right)} \qquad x \geq 0 \tag{3.5}$$

$$F_X(x) = \frac{\gamma\left(\frac{\nu}{2}, \frac{x}{2}\right)}{\Gamma\left(\frac{\nu}{2}\right)} \qquad x \geq 0, \tag{3.6}$$

where $\Gamma(\cdot)$ denotes the gamma function (ABRAMOWITZ; STEGUN, 1972, eq. (6.1.1)) and $\gamma(\cdot,\cdot)$ the lower incomplete gamma function (OLVER et al., 2010, eq. (8.2.1)). Figure 3.3 shows (a) the PDF and (b) CDF of the Chi-squared distribution for multiple values of ν.

3.3.4 Weibull Distribution

It is a two parameter distribution with k and λ corresponding to shape and scale parameters, respectively. It is related to several distributions including the exponential ($k = 1$) and Rayleigh ($k = 2$ and $\lambda = \sqrt{2}\rho$) distributions. Its PDF and CDF are given by (FORBES et al., 2011):

$$f_X(x) = \frac{k}{x}\left(\frac{x}{\lambda}\right)^k \exp\left[-\left(\frac{x}{\lambda}\right)^k\right] \qquad x \geq 0 \tag{3.7}$$

$$F_X(x) = 1 - \exp\left[-\left(\frac{x}{\lambda}\right)^k\right] \qquad x \geq 0. \tag{3.8}$$

Among the many applications of the Weibull distribution (failure analysis (MARTZ, 2003), extreme value theory (MCNELIS, 2005), weather forecasting, etc.) we highlight its application in radar systems since many forms of clutter (sea, ground) can be better approximated by the Weibull distribution (SEKINE; MAO; MAO, 1990). Figure 3.4 shows the (a) PDF and (b) CDF of the Weibull distribution with scale parameter $\lambda = 2$ and multiple values of the shape parameter k.

3.3.5 Log-normal Distribution

It is a continuous probability distribution of a RV whose logarithm is normally distributed, i.e. if X is log-normally distributed then $Y = ln(X)$ follows a normal distribution (MAYMON, 2018). Therefore a RV that follows a log-normal distribution is constrained by zero resulting results in an asymmetrical and positively skewed distribution.

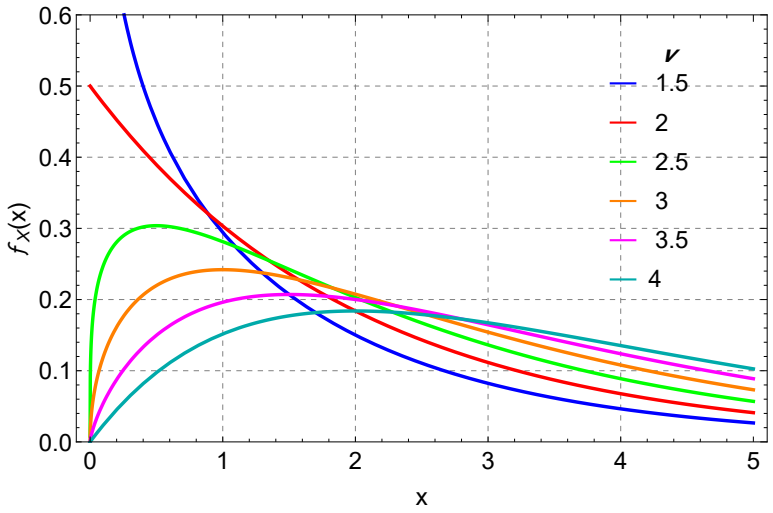

(a)

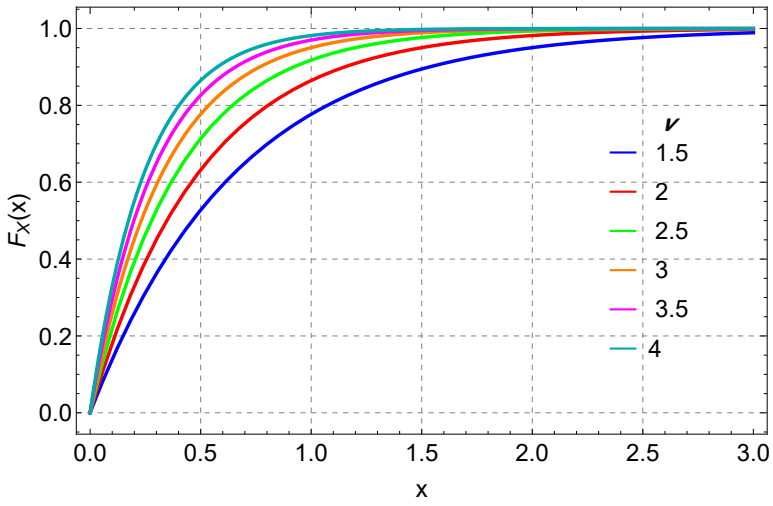

(b)

Figure 3.3 – The (a) PDF and (b) CDF of the Chi-squared distribution for multiple values of ν.

Its PDF and CDF are given by (FORBES et al., 2011):

$$f_X(x) = \frac{1}{x\,\sigma\sqrt{2\pi}} \exp\left[-\frac{(\ln(x)-\mu)^2}{2\sigma^2}\right] \qquad x \geq 0 \tag{3.9}$$

$$F_X(x) = \frac{1}{2}\left[1 + \operatorname{erf}\left(\frac{\ln(x)-\mu}{\sqrt{2}\sigma}\right)\right] \qquad x \geq 0, \tag{3.10}$$

where $\operatorname{erf}(\cdot)$ denotes the error function (OLVER et al., 2010, eq. (7.2.1)), μ and σ correspond to the expected value and standard deviation respectively, of the variable's natural logarithm. The log-normal distribution is used to model: weight of adults, concentration of mineral deposits, distribution of wealth, among others (FORBES et al., 2011). Figure 3.5 shows the (a) PDF and (b) CDF of the log-normal distribution for $\sigma = 0.4$ and multiple values of μ.

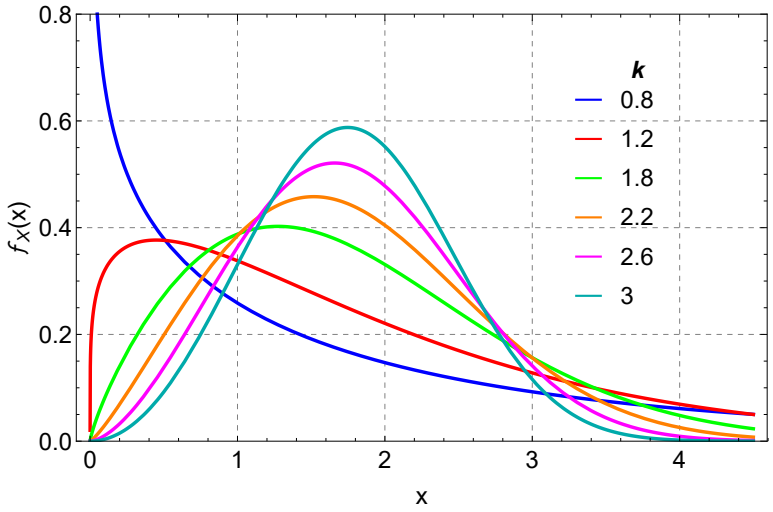

(a)

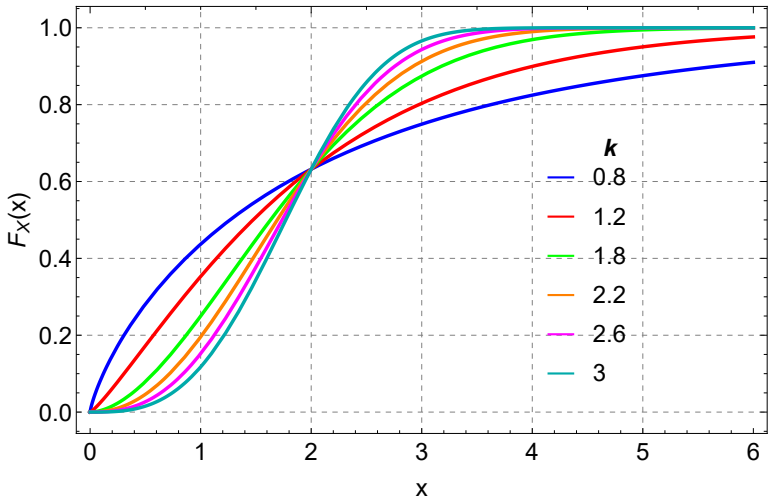

(b)

Figure 3.4 – The (a) PDF and (b) CDF of the Weibull distribution with $\lambda = 2$ for multiple values of k.

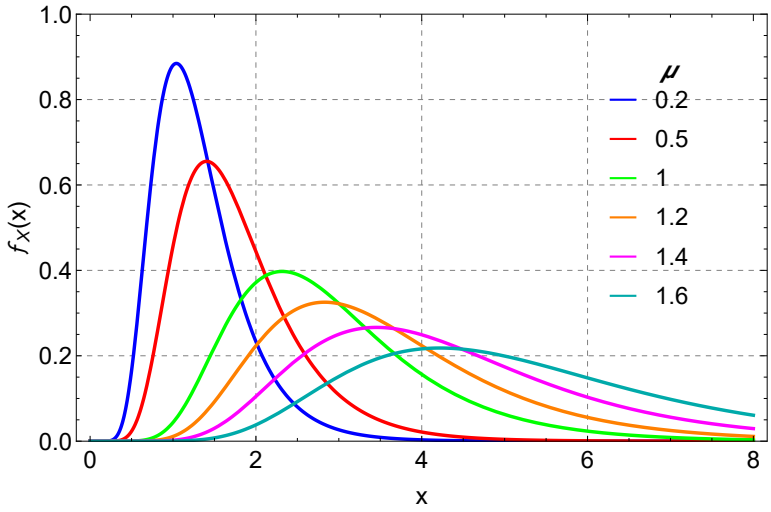

(a)

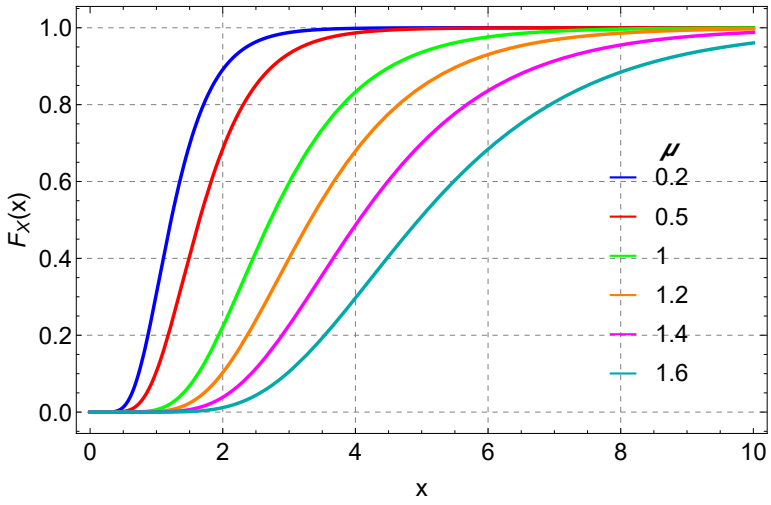

(b)

Figure 3.5 – The (a) PDF and (b) CDF of the log-normal distribution with $\sigma = 0.4$ and for multiple values of μ.

4 Constant False Alarm Rate

As described in Section 2.1.1 the NP criterion maximizes the PD given a desired PFA. The NP detector is used assuming that the interference is independent and identically distributed (i.i.d.) and that the parameters of the distribution are known (which generally is not the case). In realistic scenarios this criterion leads to increasing false alarm rates degrading the detector's performance. Thus, it is imperative to employ a detector that uses the measured data to estimate the distribution parameters and makes use of such estimate to compute the detector's threshold. A property of such detector will be the ability to maintain a fixed PFA in the presence of heterogeneous interference. This detector is know as a constant false alarm rate detector and its generic architecture is shown in Figure 4.1.

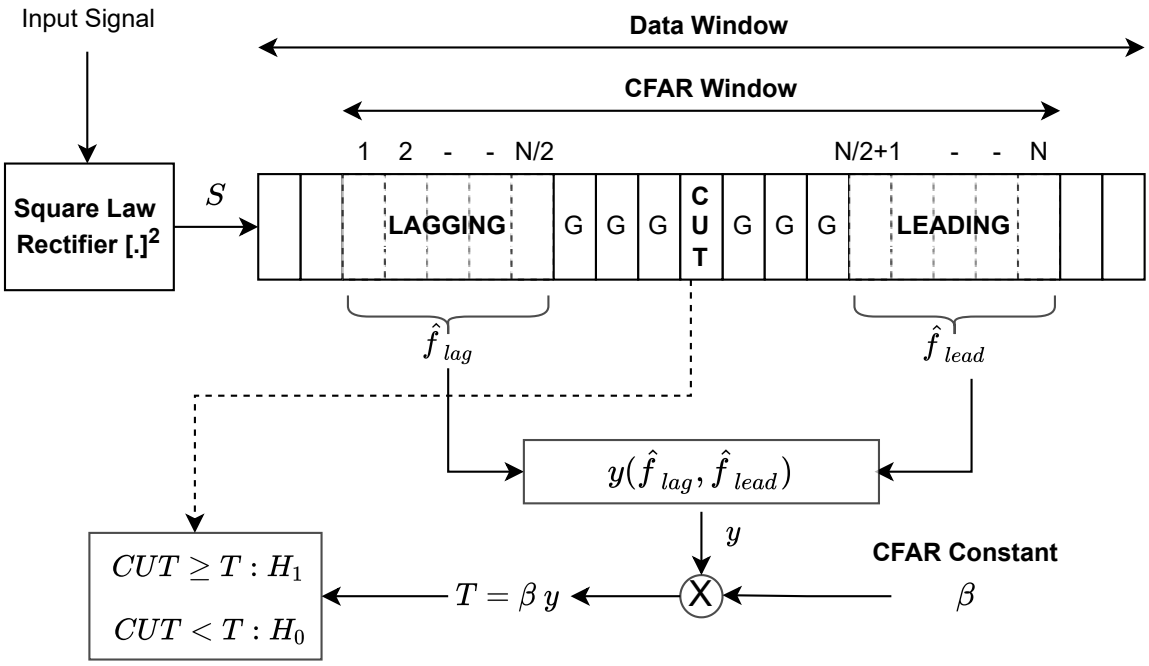

Figure 4.1 – Generic architecture of a CFAR detector.

As depicted the samples at the rectifier's output are stored as a one dimensional vector called data window. The CFAR window resides within the data window and is composed of leading and lagging windows (often called reference windows), each containing the same number of cells ($N/2$). The reference window is defined outside the guard cell region (denoted by "G"). The CFAR windows moves across the data windows one cell at a time, therefore all available data is tested for the presence of a target. The current cell under test (CUT) is compared against a threshold which is determined by the interference statistic. The algorithm estimates the interference statistic from the samples residing in reference window only since the guard cells may contain returns associated with the target

in the CUT. As seen in Figure 4.1, some CFAR algorithms process the leading and lagging windows separately computing individual statistics ($\hat{f}_{lag}$ and $\hat{f}_{lead}$) to then combine them resulting in a composite statistic y (RICHARDS et al., 2010).

Because of the uncertainties in the CFAR statistic the threshold needed for a fixed PFA is greater than the one associated with the NP detector. This is equivalent to a higher SNR which is interpreted as "loss". Thus, the ratio between the SNR required by the CFAR detector to that of the NP detector is termed as CFAR loss (RICHARDS et al., 2010).

In heterogeneous environments, both changes in the background interference and multiple targets degrade the CFAR performance. This conditions occur respectively when: target returns that are present in the reference windows bias the threshold estimate making the target in the CUT undetectable (target masking); and, localized sharp changes in the interference power (clutter boundaries) that increase false alarms and masks targets that are located near the boundary. In the following sections we address some of the most popular CFAR algorithms that are design to work in either homogeneous or heterogeneous environments (RICHARDS et al., 2010).

4.1 Cell Averaging CFAR

The cell averaging CFAR (CA-CFAR), proposed by (FINN, 1968), computes the threshold (T) by estimating the average interference power in the reference windows. It is design to operate in homogeneous environments meaning that it is assumed that the interference in the CUT and reference windows is i.i.d.; and, that leading and lagging windows do not contain returns from targets when one is present at the CUT. It is important to mention that CFAR detectors achieve a constant false alarm rate without a priori knowledge of the interference power. This is know as the CFAR property and is derived from the PFA being independent of the interference power. Also, references to the PD and PFA in the performance of a CFAR detector denote average probability which is obtained by integrating over all possible values of the interference statistic (RICHARDS et al., 2010).

4.2 Greatest-of CA-CFAR

In order to reduce clutter edge false alarms the greatest-of CA-CFAR (GOCA-CFAR) was introduce by (HANSEN; SAWYERS, 1980). The algorithm computes the average interference power in the reference windows separately to then select the larger of the two sample mean as the CFAR statistic. The GOCA-CFAR bias the threshold above the clutter edge and therefore reduces the occurrence of false alarms. It exhibits degraded

performance in the presence of interfering targets (RICHARDS et al., 2010).

4.3 Smallest-of CA-CFAR

The smallest-of CA-CFAR (SOCA-CFAR) was proposed by (TRUNK, 1978) to address mutual target masking. It estimates the interference in leading and lagging windows separately to then select the smaller of the two estimates as the CFAR statistic. It suppress interfering targets that are present in either lagging or leading windows but not both (RICHARDS et al., 2010).

4.4 Censored CFAR

The censored CFAR (CS-CFAR) was introduced by (RICKARD; DILLARD, 1977a; RITCEY, 1986a). It rank orders the measured samples in the leading and lagging windows to then discard the largest N_C samples. The CFAR statistic is then estimated by averaging the remaining samples in the reference window. The N_C samples are discarded because they are believe to contain returns from interfering targets. Thus, the CS-CFAR is capable of removing N_C interfering targets that could bias the detector. It is important to mention that the user is required to determine, a priori, the maximum number of interference targets present at the reference window (RICHARDS et al., 2010).

4.5 Order Statistics CFAR

The order statistics CFAR (OS-CFAR) is design to suppress target masking (ROHLING, 1983; ROHLING, 1985). To do so, the algorithm rank orders the N samples in the reference window forming a new sequence. The k-th element of the ordered sequence (known as the k-th order statistic) is selected as the CFAR statistic. For instance, the first order statistic is the minimum, the N-th order statistic is the maximum and the $N/2$-th order statistic is the mean of the data. Thus, the interference is estimated based on one data sample. Also, the algorithm is capable of rejecting $N - k$ interfering targets and suppressing clutter edge false alarms for $k > N/2$ (RICHARDS et al., 2010; RICHARDS, 2014).

It can therefore be deduced that the selection of a CFAR detector depends on environmental characteristics in which the radar is to operate. Table 4.1 shows some of the CFAR algorithms and the environments each one is design to operate in to further summarize the previous sections.

Table 4.1 – CFAR algorithms and the environment each one is design to operate in (RICHARDS et al., 2010).

CFAR	Homogeneous	Heterogeneous	Interfering Targets	Clutter Boundaries
CA	X			
GOCA		X		X
SOCA		X	X	
CS		X	X	
OS		X	X	X

5 SOCA-CFAR Detector Performance in Weibull-Distributed Clutter

This chapter is based on the paper bellow:

- M. C. Luna Alvarado, F. D. A. García, L. P. J. Jiménez, G. Fraidenraich and Y. Iano,"Performance Evaluation of SOCA-CFAR Detectors in Weibull-Distributed Clutter Environments," in *IEEE Geoscience and Remote Sensing Letters*, vol. 19, pp. 1-5, 2022, Art no. 4022505, doi: 10.1109/LGRS.2022.3152936.

5.1 Preamble

As mentioned, in modern radar systems it is desirable to maintain a CFAR while maximizing the PD. To achieve this the threshold adjust itself automatically based on the local interference to maintain a fixed PFA. The first detector to address this approach was the CA-CFAR but because of its limitations multiple CFAR detectors have been introduced since. Such detectors deal with target masking and clutter boundaries at the cost of increasing computation load, hardware complexity and CFAR loss (HANSEN; SAWYERS, 1980; TRUNK, 1978; ROHLING, 1983; ROHLING, 1985; KHALIGHI; BASTANI, 2000; GANDHI; KASSAM, 1988; RICKARD; DILLARD, 1977b; RITCEY, 1986b). Among them we highlight the SOCA-CFAR detector which circumvents one of the downsides of the CA-CFAR that significantly degrades its performance.

Many authors have analyze the performance of SOCA-CFAR detectors by deriving their performance metrics, PD and PFA, under the assumption that the interference background follows exponential, chi-squared, Pearson V and Pareto distributions (GANDHI; KASSAM, 1988; El Mashade; Al Hussaini, 1994; MEZIANI; SOLTANI, 2006; CHALABI et al., 2017). Even though data collected by high-frequency surface-wave radars (HFSWR) systems have proved that reflections from the sea, low grazing angle terrain and high resolution imagery are better modeled by Weibull distribution (WANG et al., 2021a; SONG; XIUWEN, 2020; WANG et al., 2021b); no SOCA-CFAR detectors under such clutter environments were carried out so far. Thus, the performance analysis of SOCA-CFAR detectors under Weibull distributed clutter remains unknown.

It is well know that dealing with Weibull distributed clutter represents a challenging task from the analytical viewpoint as well as in the signal processing treatment (BUCCIARELLI, 1985; García et al., 2020). For instance, in (ZHANG et al., 2019) the authors propose a new modified CFAR that operates in Weibull distributed interference which performance analysis for homogeneous and heterogeneous clutter was made solely via Monte-Carlo simulations. When working with CFAR detectors in Weibull clutter we encounter the lack of exact, manageable, and close-form solutions for the PDF and CDF of: **i)** the output of a square-law detector considering an exponential fluctuating target embedded in Weibull distributed clutter within the CUT, and **ii)** the sum of i.i.d. Weibull RVs. Despite solutions for the signal-plus-clutter statistics were derived in (GARCíA et al., 2019; García et al., 2021), they are to intricate to work with. Thus, more tractable and simpler solutions of this sum would be desired. Signal-plus-clutter statistics can be approximated in a closed-form by using well-known parameter estimation methods such as: method of moments (MM) (FILHO; YACOUB, 2006), generalized method of moments (GMM) (CHENG; BEAULIEU, 2002), maximum-likelihood estimator (MLE) (CHENG; BEAULIEU, 2001), truncated-maximum-likelihood estimator (TMLE) (AI et al., 2020), among others (BOUANANI; COSTA, 2018; COSTA; YACOUB; FILHO, 2008).

In this work capitalizing on (GARCíA et al., 2021) (which introduced novel exact expressions for the sum of i.i.d Weibull RVs) and employing the MM with the versatile $\alpha - \mu$ distribution (YACOUB, 2007) (to provide tractable and closed-form expressions for the signal-plus-clutter statistics), we will be able to evaluate the performance of SOCA-CFAR detectors in an exact and generalized manner. The analysis presented in the following sections made use of arbitrary values for the shape parameter of the Weibull interference samples contained within the CFAR window. this is in contrast to the state-of-the-art solutions that set the shape parameter value equal to one to simplify maths (GARCíA et al., 2019; ABBADI et al., 2018). The contributions of our work are summarized as follows:

1. We obtain exact expressions for the PDF and CDF for the minimum of two sums of i.i.d. Weibull RVs.

2. We provide a highly accurate closed-form approximation for the CUT's statistics of a square-law detector. To do so, we approximate the sum PDF of an exponential target and a Weibull clutter by an α–μ distribution.

3. We derive an exact expression for the PFA and an accurate closed-form approximation for the PD of a SOCA-CFAR detector operating in Weibull clutter, allowing arbitrary values for the shape parameter of the Weibull interference.

The remainder of this chapter is organized as follows. Section 5.2 revises the sum of i.i.d. Weibull RVs. Section 5.3 derives essential sum statistics that will be used throughout this letter. Section 5.5 analyzes the performance of a SOCA-CFAR detector operating over Weibull-distributed clutter. Section 6 examines significant numerical results. Finally, Section 7 discuss the main conclusions of the work.

In this fashion, $\Pr[\cdot]$ denotes probability; $f_{(\cdot)}(\cdot)$, PDF; $F_{(\cdot)}(\cdot)$, CDF; $\Gamma(\cdot)$, the gamma function (ABRAMOWITZ; STEGUN, 1972, eq. (6.1.1)); $\Gamma(\cdot,\cdot)$, the upper incomplete gamma function (OLVER et al., 2010, eq. (8.2.2)); $\mathbb{E}[\cdot]$, expectation; $\mathbb{V}[\cdot]$, variance; and $|\cdot|$, absolute value.

5.2 Preliminaries

Here we revisit the sum of N i.i.d. Weibull RVs proposed by (GARCíA et al., 2021) which aids us derive the essential statistics presented in Section 5.3.

5.2.1 Sum of i.i.d. Weibull variates

Let X_n be a Weibull RV with PDF and CDF given, respectively, by

$$f_{X_n}(x_n) = \frac{k}{x_n}\left(\frac{x_n}{\lambda}\right)^k \exp\left[-\left(\frac{x_n}{\lambda}\right)^k\right] \qquad x_n \geq 0 \tag{5.1}$$

$$F_{X_n}(x_n) = 1 - \exp\left[-\left(\frac{x_n}{\lambda}\right)^k\right], \qquad x_n \geq 0 \tag{5.2}$$

where $k > 0$ and $\lambda > 0$ are shape and scale parameters, respectively.

Now, let Z be the sum of N i.i.d. Weibull RVs X_n, i.e.,

$$Z = \sum_{n=1}^{N} X_n. \tag{5.3}$$

The PDF and CDF for the sum in (5.3) are given, respectively, by (GARCíA et al., 2021)

$$f_Z(z) = z^{-1}k^N\left(\frac{z}{\lambda}\right)^{kN}\sum_{i=0}^{\infty}\frac{\delta_i z^{ik}}{\Gamma(ik+kN)} \tag{5.4}$$

$$F_Z(z) = k^N z^{kN}\left(\frac{1}{\lambda}\right)^{kN}\sum_{i=0}^{\infty}\frac{\delta_i z^{ik}}{\Gamma(ik+Nk+1)}, \tag{5.5}$$

where δ_i are coefficients that can be obtained recursively by

$$\delta_0 = \Gamma(k)^N \tag{5.6a}$$

$$\delta_i = \frac{1}{i\,\Gamma(k)}\sum_{l=1}^{i}\frac{\delta_{i-l}\,(lN+l-i)\,\Gamma(lk+k)\left(-\left(\frac{1}{\lambda}\right)^k\right)^l}{l!}. \tag{5.6b}$$

Figures 5.1 and 5.2 show the PDF and CDF regarding the sum of N i.i.d. Weibull RVs address in equations (5.4) and (5.5).

5.3 Some Important Statistics

In this section, capitalizing on (GARCíA et al., 2021), we obtain exact formulations for the PDF and CDF of the minimum of two sums of N i.i.d. Weibull variates. Also, we approximate the sum PDF of an exponential and a Weibull RV by the $\alpha - \mu$ distribution.

5.3.1 Minimum of Two Sums of i.i.d. Weibull variates

Proposition 1. *Let Y be the minimum of two sums of N i.i.d. Weibull RVs, i.e.,*

$$Y = min(Z_1, Z_2), \tag{5.7}$$

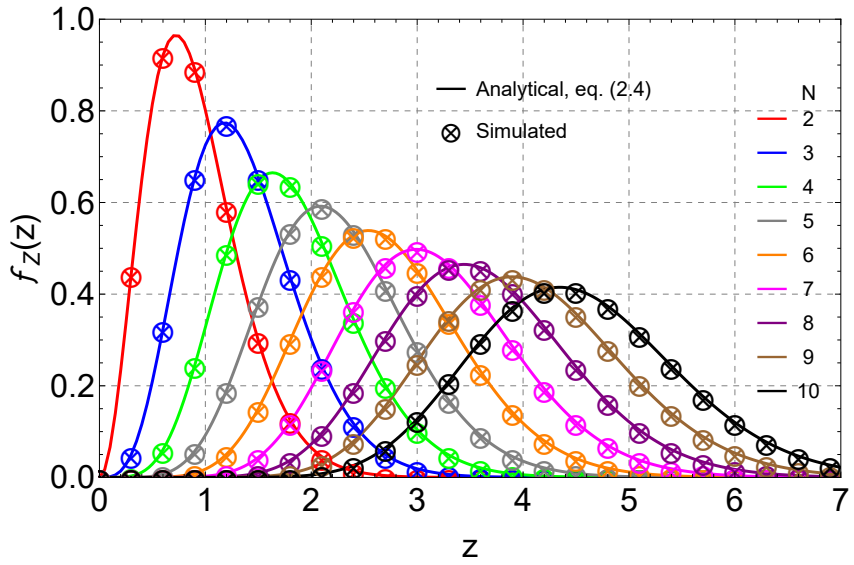

Figure 5.1 – PDF of Z for multiple values of N.

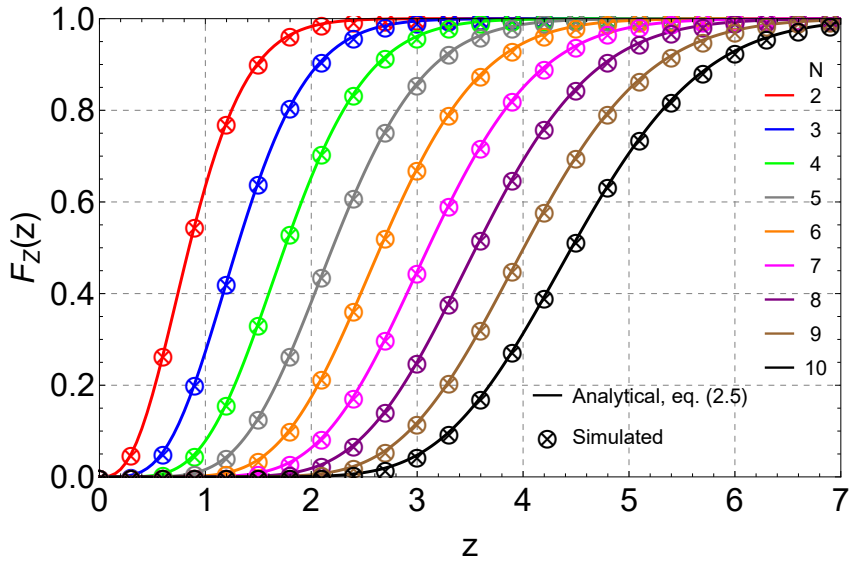

Figure 5.2 – CDF of Z for multiple values of N.

in which

$$Z_1 = \sum_{n=1}^{N} A_n, \qquad Z_2 = \sum_{n=1}^{N} B_n, \tag{5.8}$$

where A_n and B_n are i.i.d. Weibull RVs with PDF given by (5.1). Then, the PDF and CDF of Y are given, respectively, by

$$f_Y(y) = \frac{2k^N}{y}\left(\frac{y}{\lambda}\right)^{kN} \sum_{i=0}^{\infty} y^{ik}\left[\frac{\delta_i}{\Gamma(ik+Nk)} - d_i\, k^N \left(\frac{y}{\lambda}\right)^{kN}\right] \tag{5.9}$$

$$F_Y(y) = \frac{2k^N y^{kN}}{\lambda^{kN}} \sum_{i=0}^{\infty} y^{ik}\left[\frac{\delta_i}{\Gamma(ik+kN+1)} - \frac{d_i\, k^N \left(\frac{y}{\lambda}\right)^{kN}}{k(i+2N)}\right], \tag{5.10}$$

where the coefficients d_i can be obtained recursively from

$$d_i = \sum_{m=0}^{i} \frac{\delta_m}{\Gamma(km+kN)} \frac{\delta_{i-m}}{\Gamma(1+k(i-m+N))}, \qquad i \geq 0. \tag{5.11}$$

Proof. As well known, the PDF and CDF for minimum of Z_1 and Z_2 can be written, respectively, as (PAPOULIS; PILLAI, 2002)

$$f_Y(y) = f_{Z_1}(y)\,(1 - F_{Z_2}(y)) + f_{Z_2}(y)\,(1 - F_{Z_1}(y)) \tag{5.12}$$

$$F_Y(y) = F_{Z_1}(y) + F_{Z_2}(y) - F_{Z_1}(y)F_{Z_2}(y). \tag{5.13}$$

Since $f_{Z_1}(y) = f_{Z_2}(y)$ and $F_{Z_1}(y) = F_{Z_2}(y)$, (5.12) and (5.13) can be written as

$$f_Y(y) = 2f_{Z_1}(y) - 2f_{Z_1}(y)F_{Z_1}(y) \tag{5.14}$$

$$F_Y(y) = 2F_{Z_1}(y) - F_{Z_1}(y)^2. \tag{5.15}$$

Substituting (5.4) and (5.5) into (5.14) we obtain

$$f_Y(y) = \frac{2k^N}{y}\left(\frac{y}{\lambda}\right)^{kN}\left[\sum_{i=0}^{\infty}\frac{\delta_i\, y^{ik}}{\Gamma(ik+Nk)} - k^N\left(\frac{y}{\lambda}\right)^{kN}\left(\sum_{i=0}^{\infty}\frac{\delta_i y^{ik}}{\Gamma(ik+Nk)}\right)\left(\sum_{i=0}^{\infty}\frac{\delta_i y^{ik}}{\Gamma(ik+Nk+1)}\right)\right]. \tag{5.16}$$

Now, employing Cauchy's product of two infinite series we get

$$f_Y(y) = \frac{2k^N}{y}\left(\frac{y}{\lambda}\right)^{kN}\left[\sum_{i=0}^{\infty}\frac{\delta_i\, y^{ik}}{\Gamma(ik+Nk)} - k^N\left(\frac{y}{\lambda}\right)^{kN}\sum_{i=0}^{\infty} d_i\, y^{ik}\right], \tag{5.17}$$

and after further simplifications we yield in (5.9). Regarding $F_Y(y)$, since we have $f_Y(y)$ we simply integrate (5.9) from 0 to y to obtain (5.10). ■

5.3.2 Clutter-Plus-Target Statistics

Proposition 2. *Let P and W be an exponential and a Weibull RV, respectively, with PDFs given by*

$$f_P(p) = \hat{\eta}\exp(-\hat{\eta}\,p) \qquad p \geq 0 \tag{5.18}$$

$$f_W(w) = \frac{\hat{k}}{w}\left(\frac{w}{\hat{\lambda}}\right)^{\hat{k}}\exp\left[-\left(\frac{w}{\hat{\lambda}}\right)^{\hat{k}}\right], \qquad w \geq 0 \tag{5.19}$$

where $\hat{\eta} > 0$ represents the rate parameter of the exponential distribution, whereas $\hat{k} > 0$ and $\hat{\lambda} > 0$ correspond to the shape and scale parameters of the Weibull distribution. Then, the sum PDF and CDF of $\Phi = P + W$ can be accurately approximated by an $\alpha - \mu$ distribution (YACOUB, 2007) with PDF and CDF given, respectively, by

$$f_{\hat{\Phi}}(\hat{\phi}) = \frac{\alpha\,\mu^{\mu}\hat{\phi}^{\alpha\mu-1}}{\Omega^{\mu}\Gamma(\mu)}\exp\left(-\frac{\mu\,\hat{\phi}^{\alpha}}{\Omega}\right) \tag{5.20}$$

$$F_{\hat{\Phi}}(\hat{\phi}) = 1 - \frac{\Gamma\left(\mu, \frac{\mu\,\hat{\phi}^{\alpha}}{\Omega}\right)}{\Gamma(\mu)}, \tag{5.21}$$

where $\alpha > 0$ *is the shape parameter,* $\Omega = \mathbb{E}[\hat{\Phi}^\alpha]$ *is the scale parameter, and* $\mu = \mathbb{E}^2\left[\hat{\Phi}^\alpha\right]/\mathbb{V}\left[\hat{\Phi}^\alpha\right] > 0$ *is the inverse of the normalized variance of* $\hat{\Phi}^\alpha$.

Proof. To render a good approximation, we made use of the $\alpha - \mu$ distribution as it is a versatile and general statistical model that comprises the Rayleigh, Exponential, one-sided Gaussian, and Weibull distributions.

To calculate the PDF parameters of the $\alpha - \mu$ distribution, we employed a moment-based approach. Specifically, the parameters μ, α, and Ω can be obtained by solving the following set of equations

$$\frac{\Gamma^2\left(\mu + \frac{1}{\alpha}\right)}{\Gamma(\mu)\Gamma\left(\mu + \frac{2}{\alpha}\right) - \Gamma^2\left(\mu + \frac{1}{\alpha}\right)} = \frac{\mathbb{E}^2[\hat{\Phi}]}{\mathbb{E}\left[\hat{\Phi}^2\right] - \mathbb{E}^2[\hat{\Phi}]} \tag{5.22}$$

$$\frac{\Gamma^2\left(\mu + \frac{2}{\alpha}\right)}{\Gamma(\mu)\Gamma\left(\mu + \frac{4}{\alpha}\right) - \Gamma^2\left(\mu + \frac{2}{\alpha}\right)} = \frac{\mathbb{E}^2\left[\hat{\Phi}^2\right]}{\mathbb{E}\left[\hat{\Phi}^4\right] - \mathbb{E}^2\left[\hat{\Phi}^2\right]} \tag{5.23}$$

$$\Omega = \left[\frac{\mu^{1/\alpha}\,\Gamma(\mu)\,\mathbb{E}[\hat{\Phi}]}{\Gamma\left(\mu + \frac{1}{\alpha}\right)}\right]^\alpha, \tag{5.24}$$

where the moments of $\hat{\Phi}$ can be computed through multinomial expansion as

$$\mathbb{E}\left[\hat{\Phi}^n\right] = \sum_{m=0}^{n} \binom{n}{m} \mathbb{E}\left[P^{n-m}\right] \mathbb{E}\left[W^m\right], \tag{5.25}$$

in which n is a positive integer. On the other hand, the moments for P and W can be computed, respectively, by

$$\mathbb{E}\left[P^n\right] = \frac{n!}{\hat{\eta}^n} \tag{5.26}$$

$$\mathbb{E}\left[W^n\right] = \hat{\lambda}^n\,\Gamma\left(1 + \frac{n}{\hat{k}}\right). \tag{5.27}$$

This completes the proof. ■

5.4 The $\alpha - \mu$ Distribution

The $\alpha - \mu$ is a general fading distribution. It is very versatile and mathematically tractable. It includes the Gamma, Weibull, Nakagami-m, exponential, one-sided Gaussian and Rayleigh distributions. The Weibull distribution can be obtained by setting $\mu = 1$. Likewise, by setting $\mu = 1$ and $\alpha = 2$ and $\alpha = 1$ the Rayleigh and exponential distributions can be obtained, respectively. Also, by setting $\alpha = 2$ and $\mu = 1/2$ the one-sided Gaussian distribution is obtained (YACOUB, 2007). Figures 5.3 and 5.3 show the PDF and CDF of the $\alpha - \mu$ distribution alongside the distributions that it includes.

The way in which the parameters of the $\alpha - \mu$ distribution are related to the distributions it includes is as follows: Weibull distribution $k = \alpha$ and $\lambda = \Omega^{1/\alpha}$, exponential

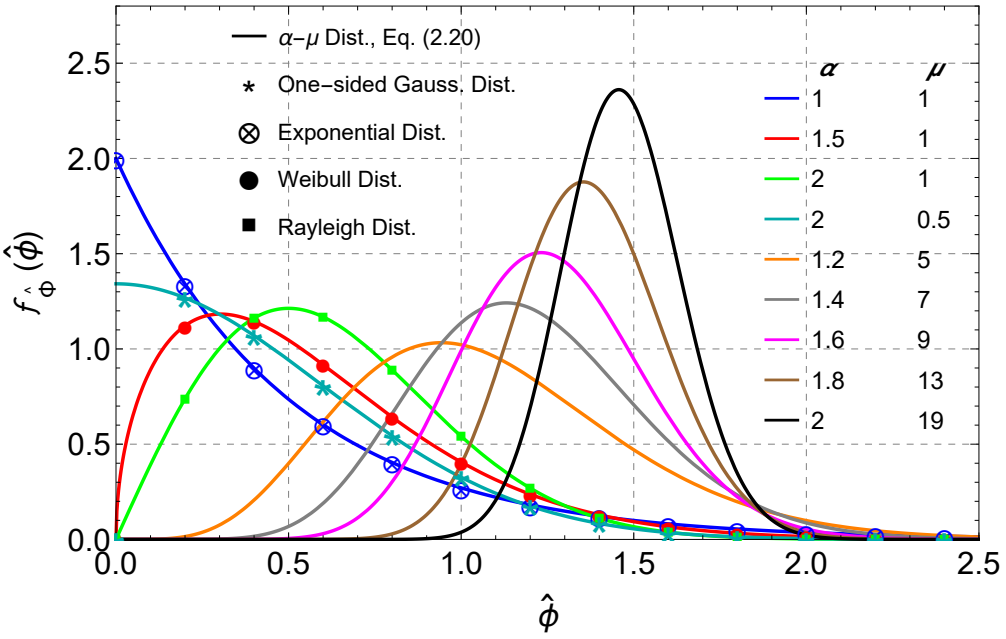

Figure 5.3 – PDF of $\alpha - \mu$ distribution for multiple values of α, μ and with $\Omega = \sqrt{\mu/4}$.

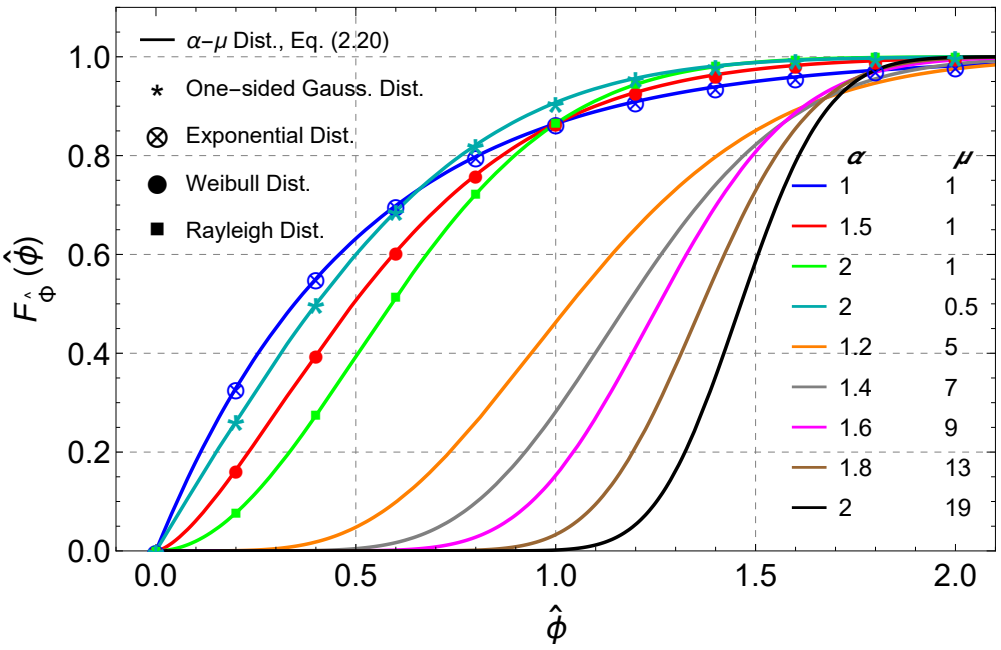

Figure 5.4 – CDF of $\alpha - \mu$ distribution for multiple values of α, μ and with $\Omega = \sqrt{\mu/4}$.

distribution $\eta = 1/\Omega$, Rayleigh distribution $\rho = \sqrt{\Omega/2}$ and one-sided Gaussian distribution $\sigma = \sqrt{\Omega}$.

5.5 SOCA-CFAR Detection

In this section, we derive the PD and PFA of a SOCA-CFAR detector operating over Weibull distributed clutter.

5.5.1 SOCA-CFAR Performance Analysis

Let W be the sample power within the CUT containing only clutter returns with PDF given by (5.19). Thus, the PFA of a SOCA-CFAR detector can be calculated by (RICHARDS et al., 2010)

$$\begin{aligned} P_{\text{FA}} &\triangleq \int_0^\infty \Pr\left[W > \frac{\beta\, y}{N}\middle| Y = y\right] f_Y(y)\,\mathrm{d}y \\ &= \int_0^\infty \int_{\beta y/N}^\infty f_W(w) f_Y(y)\,\mathrm{d}w\,\mathrm{d}y, \end{aligned} \tag{5.28}$$

where β is the scaling factor selected to maintain a required probability of false alarm, and Y is the minimum of two sum of N i.i.d. Weibull variates.

Replacing (5.9) and (5.19) into (5.28), solving the inner integral, and after lengthy algebraic manipulations, the integral in (5.28) reduces to

$$\begin{aligned} P_{\text{FA}} = \frac{2\,k^N}{\hat{k}\,\lambda^{2kN}} \left(\frac{\hat{\lambda}N}{\beta}\right)^{kN} \sum_{i=0}^{\infty} \Bigg\{ \left(\frac{\hat{\lambda}N}{\beta}\right)^{ik} \Bigg[\frac{\Gamma\left(k(i+N)/\hat{k}\right)}{\Gamma(k(i+N))} \\ \times\, \delta_i\, \lambda^{kN} - d_i\, k^N \left(\frac{\hat{\lambda}N}{\beta}\right)^{kN} \Gamma\left(\frac{k(i+2N)}{\hat{k}}\right) \Bigg] \Bigg\}. \end{aligned} \tag{5.29}$$

It can be shown that (5.29) absolutely converges if $\hat{k} = k$ which is address in Appendix A. Thus, considering $\hat{k} = k$ and assuming $\hat{\lambda} = \lambda$ equation (5.29) reduces to

$$\begin{aligned} P_{\text{FA}} = \frac{2\,k^N}{k} \left(\frac{N}{\beta}\right)^{kN} \sum_{i=0}^{\infty} \Bigg\{ \left(\frac{\lambda N}{\beta}\right)^{ik} \Bigg[\frac{\delta_i\,\Gamma(i+N)}{\Gamma(k(i+N))} \\ - d_i\, k^N \left(\frac{N}{\beta}\right)^{kN} \Gamma(i+2N) \Bigg] \Bigg\}. \end{aligned} \tag{5.30}$$

Let Φ be the sample power within the CUT containing both clutter and target returns with PDF given by (5.20). Thus, the PD of a SOCA-CFAR detector can be calculated by (RICHARDS et al., 2010)

$$\begin{aligned} P_{\text{D}} &\triangleq \int_0^\infty \Pr\left[\hat{\Phi} > \frac{\beta\, y}{N}\middle| Y = y\right] f_Y(y)\,\mathrm{d}y \\ &= \int_0^\infty \int_{\beta y/N}^\infty f_{\hat{\Phi}}(\hat{\phi}) f_Y(y)\,\mathrm{d}\hat{\phi}\,\mathrm{d}y, \end{aligned} \tag{5.31}$$

where $f_\Phi(\phi)$ is PDF of Φ given in (5.20).

Replacing (5.9) and (5.20) into (5.31) and after evaluating the inner integral, we get

$$P_{\text{D}} = \frac{1}{\Gamma(\mu)} \int_0^\infty \Gamma\left(\mu, \frac{\mu}{\Omega}\left(\frac{y\beta}{N}\right)^{\alpha}\right) f_Y(y)\,\mathrm{d}y. \tag{5.32}$$

Finally, after several mathematical manipulations, (5.32) reduces to

$$P_{\mathrm{D}} = \frac{2\,k^N}{\Gamma(\mu)\,\lambda^{kN}} \sum_{i=0}^{\infty} \left\{ \frac{\delta_i \Gamma\left(\frac{ik+Nk}{\alpha}+\mu\right)\left(\left(\frac{\beta}{N}\right)^{\alpha}\frac{\mu}{\Omega}\right)^{-\frac{k(i+N)}{\alpha}}}{\Gamma(1+ik+Nk)} - \frac{d_i k^N \Gamma\left(\frac{ik+2Nk}{\alpha}+\mu\right)\left(\left(\frac{\beta}{N}\right)^{\alpha}\frac{\mu}{\Omega}\right)^{-\frac{k(i+2N)}{\alpha}}}{\lambda^{kN}\,k(i+2N)} \right\}. \tag{5.33}$$

The absolute convergence of (5.33) is addressed in Appendix B. Eqs. (5.30) and (5.33) are the main contributions of this letter.

6 Results and Discussion

In this chapter, we validate our expressions through Monte-Carlo simulations with the number of realizations set to 10^6.

6.1 Software

It is important to mention that we made use of the software MATHEMATICA (Wolfram Research, Inc., 2021) throughout this work. It aid us derived the analytical formulations and perform simulations to validate our findings.

6.2 Monte-Carlo Simulations

Monte-Carlo simulation is a mathematical technique used to estimate the possible outcomes of an event. Generally speaking, is a technique that uses randomly generated numbers to solve any problem (THOMOPOULOS, 2013; KROESE; TAIMRE; BOTEV, 2013). For the particular case of detection, we generate a RV (which can be the result of a mathematical operation between several RVs) that follow a certain probability distribution and compare every sample of the RV to a numerical threshold (KAY, 1998).

6.3 Numerical Results

Figs. 6.1 and 6.2 respectively show both the analytical and simulated PDF and CDF of Y for different values of N. Note the perfect agreement between our derived expressions and the Monte-Carlo simulations where every analytical result matches perfectly with the simulated values.

Now to objectively evaluate whether (5.20) provides a good approximation, a goodness-of-fit test was performed using the function *DistributionFitTest[data, dist]* implemented in MATHEMATICA. The function performs a goodness-of-fit test of choice in which the null hypothesis (H_0) is associated with the statement that *data* was drawn from a population with distribution *dist* as opposed to the alternative hypothesis (H_a) that it was not. Within the possible results reported by the test we highlight: *test statistic*, which measures the difference between a sample of data and H_0 (maximum "distance"); *p-value*, denoted by p, that represents the probability of obtaining a test statistic at least as extreme as the one we actually observed; and, *significance level* of the test denoted by ϵ_j which allow us to reject H_0 when $\epsilon_j > p$ (BIAU; JOLLES; PORCHER, 2010).

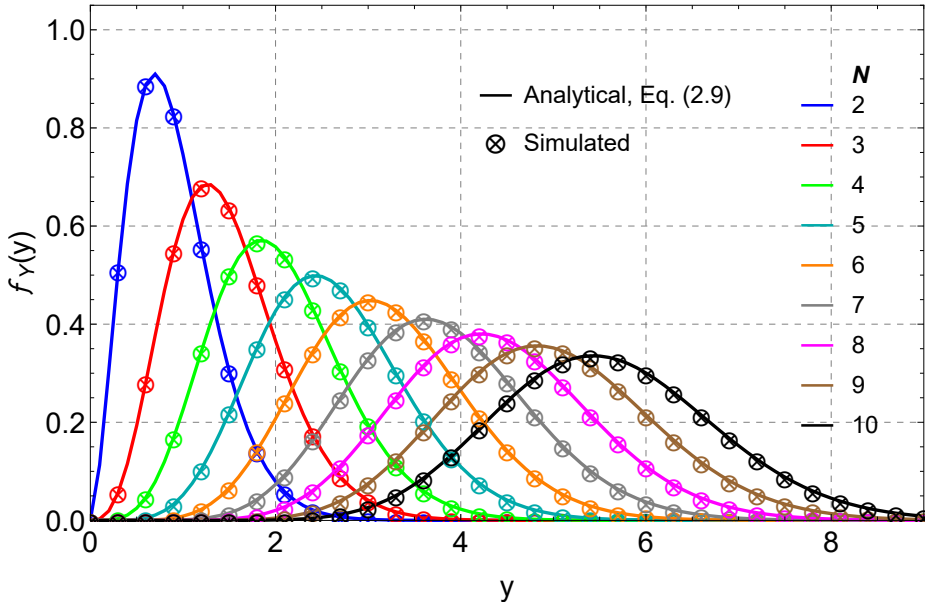

Figure 6.1 – PDF of Y considering $k = 1.3$, $\lambda = 0.7$, and different values of N.

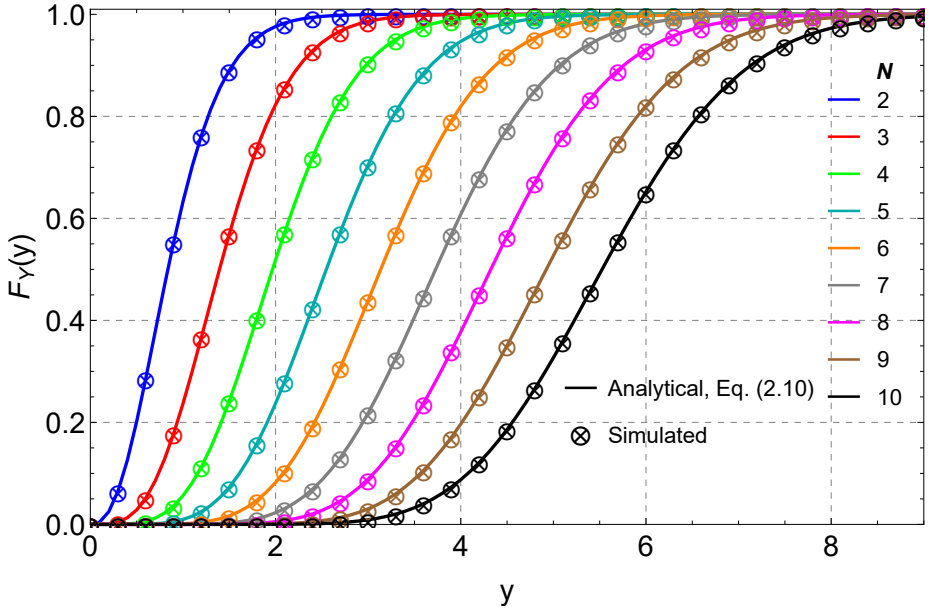

Figure 6.2 – CDF of Y considering $k = 1.3$, $\lambda = 0.7$, and different values of N.

To evaluate (5.20) as a good approximation we used the Kolmogorov-Smirnov test and its results are shown in Table 6.1. Since the *p-value* is greater than every level of significance ($\epsilon_j < p$), we are not allowed to reject the hypothesis H_0 meaning that it is likely that (5.20) was drawn from a population that follows the PDF of Φ. Moreover, since p is between 0.1 and 0.9 there is no reason to suspect the tested hypothesis is incorrect (FISHER, 1992). Therefore with $p = 0.717637$ we retain H_0 and accept it as true. Also, Fig. 6.3 illustrates the probability plot for the CDF Φ.[1] Notice that the simulated data

[1] A probability plot is a graphical tool for determining whether a data set follows a hypothesized distribution or not. The data is plotted against the theoretical distribution in such way that if the data points lie in a straight line is reasonable to assume that the samples come from the specified

Table 6.1 – Kolmogorov-Smirnov goodness-of-fit test for (5.20).

Detail	Result
Test Statistic	0.0502
P-value	0.717637
Test conclusion for $\epsilon_1 = 0.05$	Do not reject
Test conclusion for $\epsilon_2 = 0.01$	Do not reject
Test conclusion for $\epsilon_3 = 0.001$	Do not reject

for the CDF of Φ, $F_\Phi(\phi)$, closely follows the approximated CDF of Φ, $F_{\hat{\Phi}}(\hat{\phi})$ – obtained with (5.21) –. This occurs since the majority of points lie on the reference red line or in its proximities, thereby corroborating the accuracy of (5.21). Moreover, Figure 6.4 shows that the PDF in (5.20) is an excellent approximation for the sum PDF of Φ, showing an almost perfect agreement with Monte-Carlo simulations for multiple parameter settings.

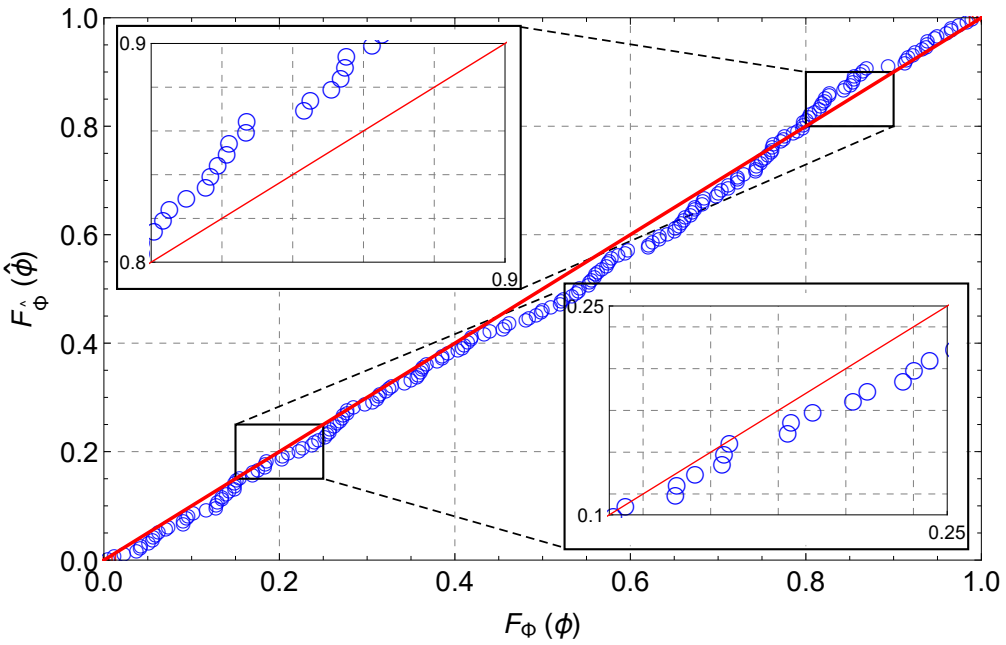

Figure 6.3 – Probability plot of (5.21) versus the simulated CDF of Φ with distribution parameters $\hat{\eta} = 0.5$, $\hat{k} = 1.3$, $\hat{\lambda} = 0.7$ and estimated parameters $\alpha = 0.70$, $\mu = 3.38$, and $\Omega = 1.87$.

Fig. 6.5 shows both the analytical and simulated PD as a function of the PFA for different values of N. Notice that as the number of random variables N increases, so does the PD as expected. Fig. 6.6 shows the analytical and simulated PD versus PFA but considering different values of the shape parameter k. Observe that the system performance improves as the shape parameter of the Weibull interference increases. Moreover, notice in both figures that the proposed approximation accurately fits the CUT's statistics.

distribution (FERRé, 2009).

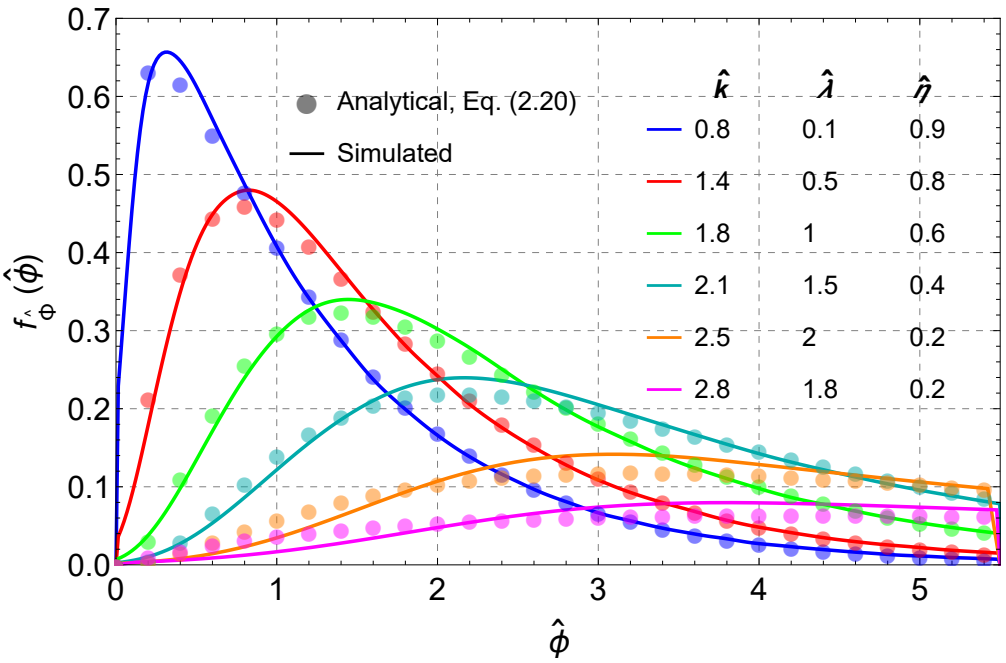

Figure 6.4 – Approximated PDF (5.20) versus simulated PDF of Φ for multiple values of parameters $\hat{\eta}$, $\hat{k}$, and $\hat{\lambda}$.

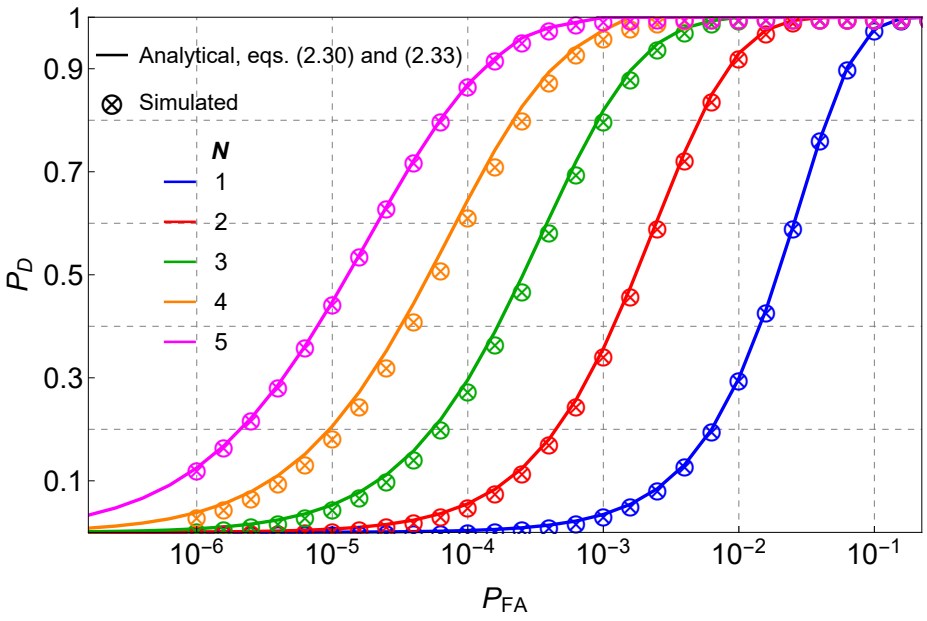

Figure 6.5 – PD versus PFA with $\hat{k} = 20$, $\hat{\lambda} = 6$, $\hat{\eta} = 12$, and considering $k = 2$, $\lambda = 1$ for multiple values of N.

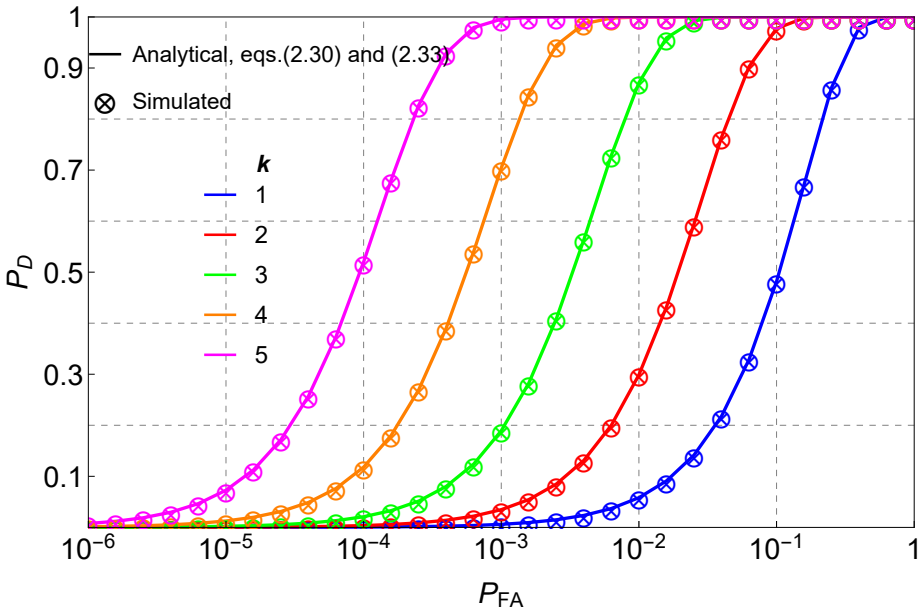

Figure 6.6 – PD versus PFA with $\hat{k} = 20$, $\hat{\lambda} = 6$, $\hat{\eta} = 12$, and considering $N = 1$, $\lambda = 1$ for different values of k.

7 Conclusions

In this work, we derived an exact expression for the PFA and an approximate closed-form solution for the PD of a SOCA-CFAR detector operating over Weibull-distributed clutter environments. The expressions derived herein can aid in the design and analysis of SOCA-CFAR detectors in more realistic clutter scenarios and, more importantly, can be easily computed using well-known mathematical packages. Numerical results indicate that the system performance improves as N or k increases. In addition, we obtained exact expressions for the PDF and CDF of the minimum of two sums of i.i.d. Weibull variates which aids us derive the performance metrics of the SOCA-CFAR processor.

Our contributions, are a novelty to the academic field and can gain further importance if used in field applications since the developed metrics account for Weibull distributed environments. Being this the case of ground and sea clutter, applications such as ship detection can benefit from the formulations we have obtained. This clearly leads to the design of SOCA-CFAR detectors who's performance metrics would be enhanced in more realistic clutter scenarios.

8 Future Works

Considering the outstanding results that were derived and further validated in this dissertation we could expand our research in the following manner:

- Derive, in an exact fashion, the PDF and CDF for the sum in Φ, which in itself would be a new and novel result in the literature, to then obtain the exact PD formulation for a SOCA-CFAR detector operating in i.i.d. Weibull distributed clutter.
- Derive performance metrics, namely PD and PFA, for other CFAR algorithms such as OS-CFAR, GOCA-CFAR, CS-CFAR.
- Derive performance metrics for the aforementioned CFAR algorithms when considering a non-i.i.d Weibull distributed clutter. This represents a challenge since first we will need to derive the sum of N non-i.i.d. Weibull RVs to then apply it to our analysis.

Bibliography

ABBADI, A. et al. Generalized closed-form expressions for CFAR detection in heterogeneous environment. *IEEE Geosci. Remote Sens. Lett.*, v. 15, n. 7, p. 1011–1015, 2018.

ABRAMOWITZ, M.; STEGUN, I. A. *Handbook of Mathematical Functions with Formulas, Graphs, and Mathematical Tables*. 10. ed. Washington, DC: US Dept. of Commerce: National Bureau of Standards, 1972.

AI, J. et al. Outliers-robust CFAR detector of Gaussian clutter based on the truncated-maximum-likelihood- estimator in sar imagery. *EEE Trans. Intell. Transp. Syst.*, v. 21, n. 5, p. 2039–2049, Apr. 2020.

BIAU, D. J.; JOLLES, B. M.; PORCHER, R. P value and the theory of hypothesis testing: an explanation for new researchers. *Clinical Orthopaedics and Related Research®*, Springer, v. 468, n. 3, p. 885–892, Nov. 2010.

BOUANANI, F. E.; COSTA, D. B. da. Accurate closed-form approximations for the sum of correlated Weibull random variables. *IEEE Wireless Commun. Lett.*, v. 7, n. 4, p. 498–501, Jan. 2018.

BUCCIARELLI, T. CFAR problems in Weibull clutter. *Electron. Lett.*, v. 21, n. 8, p. 286–304, Apr. 1985.

CHALABI, I. et al. CFAR detectors for MIMO radars in a Pareto background. In: *2017 Seminar on Detection Systems Architectures and Technologies (DAT)*. [S.l.: s.n.], 2017. p. 1–6.

CHENG, J.; BEAULIEU, N. Maximum-likelihood based estimation of the Nakagami m parameter. *IEEE Commun. Lett.*, v. 5, n. 3, p. 101–103, Mar. 2001.

CHENG, J.; BEAULIEU, N. Generalized moment estimators for the Nakagami fading parameter. *IEEE Commun. Lett.*, v. 6, n. 4, p. 144–146, Apr. 2002.

COSTA, D. B. da; YACOUB, M. D.; FILHO, J. C. S. S. An improved closed-form approximation to the sum of arbitrary Nakagami-m variates. *IEEE Trans. Veh. Technol.*, v. 57, n. 6, p. 3854–3858, Nov. 2008.

Chapter 15 - wind energy. In: da Rosa, A. V.; ORDóñEZ, J. C. (Ed.). *Fundamentals of Renewable Energy Processes (Fourth Edition)*. Fourth edition. Oxford: Academic Press, 2022. p. 721–794. ISBN 978-0-12-816036-7.

El Mashade, M. B.; Al Hussaini, E. K. Performance of CFAR detectors for M-sweeps in the presence of interfering targets. *Signal Processing*, v. 38, n. 2, p. 211–222, Jul. 1994. ISSN 0165-1684.

FERRé, J. 3.02 - regression diagnostics. In: BROWN, S. D.; TAULER, R.; WALCZAK, B. (Ed.). *Comprehensive Chemometrics*. Oxford: Elsevier, 2009. p. 33–89. ISBN 978-0-444-52701-1.

FILHO, J.; YACOUB, M. Simple precise approximations to Weibull sums. *IEEE Commun. Lett.*, v. 10, n. 8, p. 614–616, Aug. 2006.

FINN, H. Adaptive detection mode with threshold control as a function of spatially sampled clutter-level estimates. *RCA Rev.*, v. 29, p. 414–465, Sep. 1968.

FISHER, R. A. The arrangement of field experiments. In: *Breakthroughs in statistics*. [S.l.]: Springer, 1992. p. 82–91.

FORBES, C. et al. *Statistical distributions*. [S.l.]: Wiley Hoboken, 2011. v. 4.

GANDHI, P.; KASSAM, S. Analysis of CFAR processors in nonhomogeneous background. *IEEE Trans. Aerosp. Electron. Syst.*, v. 24, n. 4, p. 427–445, Jul. 1988.

García, F. D. A. et al. Alternative representations for the probability of detection of non-fluctuating targets. *Electron. Lett.*, v. 56, n. 21, p. 1136–1139, Oct. 2020.

García, F. D. A. et al. Square-law detection of exponential targets in Weibull-distributed ground clutter. *IEEE Geosci. Remote Sens. Lett.*, v. 18, n. 11, p. 1956–1960, Nov. 2021.

GARCíA, F. D. A. et al. Light exact expressions for the sum of Weibull random variables. *IEEE Wireless Commun. Lett.*, v. 10, n. 11, p. 2445–2449, Nov. 2021.

GARCíA, F. D. A. et al. CA-CFAR detection performance in homogeneous Weibull clutter. *IEEE Geosci. Remote Sens. Lett.*, v. 16, n. 6, p. 887–891, Jun. 2019. ISSN 1558-0571.

HANSEN, V. G.; SAWYERS, J. H. Detectability loss due to"greatest of" selection in a cell-averaging CFAR. *IEEE Trans. Aerosp. Electron. Syst.*, IEEE, n. 1, p. 115–118, Jan. 1980.

KAY, S. *Intuitive probability and random processes using MATLAB*. [S.l.]: Springer Science & Business Media, 2006.

KAY, S. M. *Fundamentals of Statistical Signal Processing: Detection Theory*. [S.l.: s.n.], 1998. v. 2.

KHALIGHI, M.; BASTANI, M. Adaptive CFAR processor for nonhomogeneous environments. *IEEE Trans. Aerosp. Electron. Syst.*, v. 36, n. 3, p. 889–897, Jul. 2000.

KREYSZIG, E. *Advanced Engineering Mathematics*. 10. ed. New Jersey: John Wiley & Sons, 2010.

KROESE, D. P.; TAIMRE, T.; BOTEV, Z. I. *Handbook of Monte Carlo methods*. [S.l.]: John Wiley & Sons, 2013.

LEVANON, N. *Radar Principles*. 1. ed. [S.l.]: Wiley, 1988.

MACKAY, E. 8.03 - resource assessment for wave energy. In: SAYIGH, A. (Ed.). *Comprehensive Renewable Energy*. Oxford: Elsevier, 2012. p. 11–77. ISBN 978-0-08-087873-7.

MARTZ, H. F. Reliability theory. In: MEYERS, R. A. (Ed.). *Encyclopedia of Physical Science and Technology (Third Edition)*. Third edition. New York: Academic Press, 2003. p. 143–159. ISBN 978-0-12-227410-7.

MAYMON, G. Chapter 2 - some important statistical distributions. In: MAYMON, G. (Ed.). *Stochastic Crack Propagation*. [S.l.]: Academic Press, 2018. p. 9–18. ISBN 978-0-12-814191-5.

MCNELIS, P. D. 2 - what are neural networks? In: MCNELIS, P. D. (Ed.). *Neural Networks in Finance*. Boston: Academic Press, 2005, (Academic Press Advanced Finance). p. 13–58.

MEZIANI, H. A.; SOLTANI, F. Performance analysis of some CFAR detectors in homogeneous and non-homogeneous Pearson-distributed clutter. *Signal Processing*, v. 86, n. 8, p. 2115–2122, Apr. 2006. ISSN 0165-1684. Special Section: Advances in Signal Processing-assisted Cross-layer Designs.

OLVER, F. W. J. et al. *NIST Handbook of Mathematical Functions*. 1. ed. Washington, DC: US Dept. of Commerce: National Institute of Standards and Technology (NIST), 2010.

PAPOULIS, A.; PILLAI, S. U. *Probability, Random Variables, and Stochastic Processes*. Fourth. Boston: McGraw Hill, 2002. ISBN 0071122567 9780071122566 0073660116 9780073660110 0071226613 9780071226615.

RICHARDS, M. A. *Fundamentals of radar signal processing*. 2. ed. [S.l.]: McGraw-Hill Education, 2014.

RICHARDS, M. A. et al. *Principles of Modern Radar: Basic Principles*. 1. ed. West Perth, WA, Australia: SciTech, 2010.

RICKARD, J. T.; DILLARD, G. M. Adaptive detection algorithms for multiple-target situations. *IEEE Transactions on Aerospace and Electronic Systems*, AES-13, n. 4, p. 338–343, Jul. 1977.

RICKARD, J. T.; DILLARD, G. M. Adaptive detection algorithms for multiple-target situations. *IEEE Trans. Aerosp. Electron. Syst.*, IEEE, AES-13, n. 4, p. 338–343, Jul. 1977.

RITCEY, J. A. Performance analysis of the censored mean-level detector. *IEEE Transactions on Aerospace and Electronic Systems*, AES-22, n. 4, p. 443–454, Jul. 1986.

RITCEY, J. A. Performance analysis of the censored mean-level detector. *IEEE Trans. Aerosp. Electron. Syst.*, IEEE, AES-22, n. 4, p. 443–454, Jul. 1986.

ROHLING, H. Radar CFAR thresholding in clutter and multiple target situations. *IEEE Trans. Aerosp. Electron. Syst.*, IEEE, AES-19, n. 4, p. 608–621, Jul. 1983.

ROHLING, H. New CFAR-processor based on an ordered statistic. In: *Proc. IEEE International Radar Conference*. [S.l.: s.n.], 1985. p. 271–275.

SEKINE, M.; MAO, Y.; MAO, Y. *Weibull radar clutter*. [S.l.]: IET, 1990.

SKOLNIK, M. I. *Introduction to Radar Systems*. Thrid. New York: McGraw Hill, 2001.

SONG, C.; XIUWEN, L. Statistical analysis of x-band sea clutter at low grazing angles. In: *2020 International Conference on Big Data Artificial Intelligence Software Engineering (ICBASE)*. [S.l.: s.n.], 2020. p. 141–144.

THOMOPOULOS, N. T. *Essentials of Monte Carlo Simulation*. New York, NY: Springer, 2013.

TRUNK, G. V. Range resolution of targets using automatic detectors. *IEEE Trans. Aerosp. Electron. Syst.*, IEEE, AES-14, n. 5, p. 750–755, Sept. 1978.

WANG, X. et al. A fast CFAR algorithm based on density-censoring operation for ship detection in SAR images. *IEEE Signal Process. Lett.*, v. 28, p. 1085–1089, May 2021.

WANG, X. et al. An automatic target detection method based on multidirection dictionary learning for HFSWR. *EEE Geosci. Remote Sens. Lett.*, p. 1–5, Mar. 2021.

Wolfram Research, Inc. *Mathematica, Version 12.3*. 2021. Champaign, IL, 2021.

YACOUB, M. D. The α-μ distribution: A physical fading model for the Stacy distribution. *IEEE Trans. Veh. Technol.*, v. 56, n. 1, p. 27–34, Jan. 2007.

YATES, R. D.; GOODMAN, D. J. *Probability and stochastic processes: a friendly introduction for electrical and computer engineers*. [S.l.]: John Wiley & Sons, 2014.

ZHANG, B. et al. A robust two-parameter CFAR detector for skywave radar ship detection. In: *2019 IEEE Radar Conference (RadarConf)*. [S.l.: s.n.], 2019. p. 1–6.

Appendix

APPENDIX A – Absolute convergence of equation (2.29)

In this section, we verify that (5.29) converges absolutely. For simplicity, let us define the following auxiliary functions:

$$\zeta_{P_{\text{FA}}}^{(i)} = \frac{1}{\Gamma(k(i+N))}\left(\frac{\hat{\lambda}N}{\beta}\right)^{ki} \tag{A.1}$$

$$\xi_{P_{\text{FA}}}^{(i)} = \lambda^{kN}\Gamma\left(\frac{k(i+N)}{\hat{k}}\right) \tag{A.2}$$

$$\vartheta_{P_{\text{FA}}}^{(i)} = k^{N}\left(\frac{N\hat{\lambda}}{\beta}\right)^{kN}\Gamma(k(i+N))\,\Gamma\left(\frac{k(i+2N)}{\hat{k}}\right). \tag{A.3}$$

If (5.29) converges absolutely, then the sum obtained by taking the absolute values of the summands in (5.29) must converge, i.e., (KREYSZIG, 2010)

$$\sum_{i=0}^{\infty}\left|\zeta_{P_{\text{FA}}}^{(i)}\left(\xi_{P_{\text{FA}}}^{(i)}\,\delta_i - \vartheta_{P_{\text{FA}}}^{(i)}\,d_i\right)\right| < \infty. \tag{A.4}$$

Due to the factor $\Gamma(lk+l)/l!$, δ_i and d_i can be either increasing (for $k \geq 1$) or decreasing (for $0 < k < 1$) functions.

For $k \geq 1$, $|\delta_i|$ $(i \geq 1)$ can be bound as

$$|\delta_i| < 2N\sum_{l=1}^{i}\frac{|\delta_{i-l}|\,\Gamma(lk+k)\left(\frac{1}{\lambda}\right)^{kl}}{l!} \tag{A.5a}$$

$$|\delta_i| = \frac{2\,\delta_0 N\left(\frac{1}{\lambda}\right)^{k\,i}\Gamma(ik+k)}{\Gamma(i)}, \tag{A.5b}$$

whether $|d_i|$ $(i \geq 1)$ can be bounded as

$$|d_i| < \frac{[(i-m)\Gamma(km+kN)]^{-1}}{m\,\Gamma(1+k\,(i-m+N))}\,4N^2 \times\sum_{l=1}^{m}\frac{|\delta_{m-l}|\,\Gamma(lk+k)\left(\frac{1}{\lambda}\right)^{kl}}{l!}\sum_{l=1}^{i-m}\frac{|\delta_{i-l-m}|\,\Gamma(lk+k)\left(\frac{1}{\lambda}\right)^{kl}}{l!} \tag{A.6a}$$

$$|d_i| = \frac{2^i\,\delta_0^2\,N^2\,\lambda^{-ik}}{\Gamma(i-1)}, \tag{A.6b}$$

where (A.5a) uses the fact that $1/\Gamma(k) < 2$ and that $|-i+l+lN| \leq iN$ for $1 \leq l \leq i$, and (A.5b) uses the last term of the summation and multiplies it by i. Likewise, (A.6a) follows the same procedure as in (A.5a) for the sums $\sum_{l=1}^{m}$ and $\sum_{l=1}^{i-m}$. Then (A.6b) uses $\Gamma(km+k)/\Gamma(km+kN) \leq 1$ and $\Gamma(k(i-m)+k)/\Gamma(1+k((i-m)+N)) \leq 1$ for $1 \leq m \leq i$ and $k \geq 1$ to later solve the sum. Also, to develop (A.5b) and (A.6b), we used the fact $|\delta_i|$ and $|d_i|$ are decreasing functions with respect to i.

Now, using the bounds (A.5b) and (A.6b) and after several algebraic manipulations we find an upper bound for (A.4) as follows

$$\sum_{i=0}^{\infty}\left|\zeta_{P_{\mathrm{FA}}}^{(i)}(\xi_{P_{\mathrm{FA}}}^{(i)}\,\delta_i-\vartheta_{P_{\mathrm{FA}}}^{(i)}\,d_i)\right| < \sum_{i=0}^{\infty}\left(\frac{\hat{\lambda}N}{\beta}\right)^{ik}\left[\Gamma\left(\frac{k(i+N)}{\hat{k}}\right)\right.$$
$$\left.\times\, 2\lambda^{kN}\frac{\delta_0(iN)\left(\frac{1}{\lambda}\right)^{ik}}{i!}+k^N\left(\frac{\hat{\lambda}N}{\beta}\right)^{kN}\Gamma\left(\frac{k(i+2N)}{\hat{k}}\right)\frac{2^i\,\delta_0^2\,N^2\,\lambda^{-ik}}{\Gamma(i-1)}\right] \tag{A.7a}$$

$$\sum_{i=0}^{\infty}\left|\zeta_{P_{\mathrm{FA}}}^{(i)}(\xi_{P_{\mathrm{FA}}}^{(i)}\,\delta_i-\vartheta_{P_{\mathrm{FA}}}^{(i)}\,d_i)\right| < \frac{2\delta_0 N^2}{\hat{\lambda}^{-\hat{k}(N+1)}}\left(\frac{N}{\beta}\right)^{\hat{k}}$$
$$\times\left[\frac{\lambda^{-\hat{k}}\,\Gamma(N)}{\left(1-\left(\frac{\hat{\lambda}N}{\beta\lambda}\right)^{\hat{k}}\right)^{N+1}}+\frac{2\,\hat{k}^N\Gamma(2(N+1))\left(\frac{N}{\beta}\right)^{\hat{k}(N+1)}}{\delta_0^{-1}\left(1-2\left(\frac{\hat{\lambda}N}{\beta\lambda}\right)^{\hat{k}}\right)^{2N+2}}\right]. \tag{A.7b}$$

Therefore, since the bound for (A.4) exists and is finite, then (5.29) converges absolutely for $k \geq 1$ provided that $\hat{k} = k$.

For $0 < k < 1$, $|\delta_i|$ $(i \geq 1)$ can be bounded as

$$|\delta_i| < N\sum_{l=1}^{i}|\delta_{i-l}|\left(\frac{1}{\lambda}\right)^{k\,l} \tag{A.8a}$$

$$|\delta_i| = \frac{\delta_0\,N\left((N+1)^i-1\right)\lambda^{-ik}}{N+1}, \tag{A.8b}$$

and $|d_i|$ $(i \geq 1)$ can be bounded as

$$|d_i| < \frac{N^2}{\Gamma(km+kN)\Gamma(k\,(i-m+N)+1)}$$
$$\times\sum_{l=1}^{m}|\delta_{m-l}|\left(\frac{1}{\lambda}\right)^{k\,l}\sum_{l=1}^{i-m}|\delta_{i-l-m}|\left(\frac{1}{\lambda}\right)^{k\,l} \tag{A.9a}$$

$$|d_i| = \frac{iN^2\,\delta_0^2\left((N+1)^{i/2}-1\right)^2\left(\frac{1}{\lambda}\right)^{ik}}{(N+1)^2\,\Gamma\left(k\left(\frac{i}{2}+N\right)\right)\Gamma\left(\frac{ik}{2}+Nk+1\right)}. \tag{A.9b}$$

To develop (A.8a) and (A.9a), we used the fact that $|-i+lN+l| \leq iN$ for $1 \leq l \leq i$, $1/\Gamma(k) < 1$ and $\Gamma(lk+k)/l! < 1$ for $0 < k < 1$, and the fact $|\delta_i|$ and $|d_i|$ are increasing functions with respect to i to obtain (A.8b) and (A.9b).

Even though the bounds for $|\delta_i|$ and $|d_i|$ exist for $0 < k < 1$, it is not possible to obtain a bound for (A.4). Hence, for $0 < k < 1$, the partial sums of (A.4) might converge but in the limit ($i \to \infty$) will diverge.

APPENDIX B – Absolute convergence of equation (2.33)

In this section, we verify that (5.33) converges absolutely. First, let us define the following auxiliary functions:

$$\zeta_{P_{\mathrm{D}}}^{(i)} = \frac{\Gamma\left(\frac{k(i+N)}{\alpha} + \mu\right)\rho^{i+N}}{\Gamma(1+ik+Nk)} \tag{B.1}$$

$$\xi_{P_{\mathrm{D}}}^{(i)} = \frac{\Gamma\left(\frac{k(i+2N)}{\alpha} + \mu\right)\rho^{i+2N}}{\lambda^{kN}\, k^{1-N}\,(i+2N)}, \tag{B.2}$$

where

$$\rho = \left(\frac{\mu\left(\frac{\beta}{N}\right)^{\alpha}}{\Omega}\right)^{-\frac{k}{\alpha}}. \tag{B.3}$$

If (5.33) converges absolutely, then the sum obtained by taking the absolute values of the summands in (5.33) must converge, i.e., (KREYSZIG, 2010)

$$\sum_{i=0}^{\infty} |\zeta_{P_{\mathrm{D}}}^{(i)}\,\delta_i - \xi_{P_{\mathrm{D}}}^{(i)}\,d_i| < \infty. \tag{B.4}$$

Considering $k \geq 1$ and using the bounds (A.5b) and (A.6b), we can find an upper bound for (5.33) as follows

$$\begin{aligned}\sum_{i=0}^{\infty} |\zeta_{P_{\mathrm{D}}}^{(i)}\,\delta_i - \xi_{P_{\mathrm{D}}}^{(i)}\,d_i| = \frac{2\delta_0 k^N}{\Gamma(\mu)\lambda^{kN}} \Bigg\{ &\frac{2\,\rho^{N-1}}{\rho^{-1} - \left(\frac{1}{\lambda}\right)^k} \\ &+ \frac{\delta_0 N k^N}{2\,k\,\rho^{2N}\,\lambda^{kN}} \Bigg[{}_2F_1\left(1; 2N; 2N+1; \frac{\rho}{\lambda^k}\right) \\ &+ {}_2F_1\left(2; 2N+1; 2N+2; \frac{\rho}{\lambda^k}\right) \frac{2\,N\,\rho}{(2N+1)\,\lambda^k} \Bigg] \Bigg\},\end{aligned} \tag{B.5}$$

where ${}_2F_1(\cdot,\cdot;\cdot;\cdot)$ is the Gauss hypergeometric function (OLVER et al., 2010, Eq. (15.1.1)).

Hence, as the bound for (B.4) exists and is finite, then (5.33) converges absolutely for $k \geq 1$ provided that $k \leq \alpha$.

Considering $0 < k < 1$ and using the bounds (A.8b) and (A.9b), we can find

and upper bound for (5.33) as

$$\sum_{i=0}^{\infty}|\zeta_{P_{\mathrm{D}}}^{(i)}\,\delta_i-\xi_{P_{\mathrm{D}}}^{(i)}\,d_i|\leq\frac{\delta_0 N k^N\left(\rho\,\lambda^{-k}\right)^{2N+1}}{k\,(N+1)^2\,\Gamma(\mu)}$$
$$\times\left[\frac{2N\,\lambda^{kN}\,\Gamma\left(\frac{k(N+1)}{\alpha}+\mu\right)}{\rho^N\,\Gamma(Nk+k)}\right.$$
$$\left.+\frac{\delta_0\,k^N\left(\sqrt{N+1}-1\right)^2\,\Gamma\left(\frac{k(2N+1)}{\alpha}+\mu\right)}{(2N+1)\,\Gamma\left(k\left(N+\frac{1}{2}\right)\right)\,\Gamma\left(Nk+\frac{k}{2}+1\right)}\right]. \tag{B.6}$$

Therefore, as the bound for (B.4) exists and is finite, then (5.33) converges absolutely for $0<k<1$ provided that $k\leq\alpha$.